Gravitational and Coriolis forces in crystal neutron interferometry. I. Theory

Gravitational and Coriolis forces in crystal neutron interferometry. I. Theory

C. P. Sasso,* G. Mana,† and E. Massa‡
INRIM–Istituto Nazionale di Ricerca Metrologica, strada delle cacce 91, 10135 Torino, Italy

(Received 1 February 2024; accepted 9 October 2024; published 20 December 2024)

The proof that neutron interference is possible using split-crystal interferometers opens the way to extended arm separation and length and to new experiments exploring quantum mechanics and gravity. Therefore, this paper reexamines the effect of gravitational and Coriolis forces on the Laue diffraction of neutrons by perfect crystals and the operation of crystal interferometers. We give in analytical form the transfer matrices for the propagation of the neutron quantum state, either pure or mixed and subjected to gravity and Coriolis force, in free space and perfect crystals. They are used to study the effect of interferometer aberrations on the quantum-mechanical phase due to the Earth's gravity. We also give an alternative way to understand the impact of gravitational and Coriolis forces in terms of the crystal displacements and tilts perceived by the neutron.

DOI: 10.1103/PhysRevA.110.062818

I. INTRODUCTION

The effect of gravity on the phase of the neutron de Broglie wave was measured by Colella [1] and subsequently in a series of experiments of increasing complexity [2–4]. These experiments used the interference between coherently split and recombined neutron waves in the Earth's gravity field. Wave splitting and recombination are obtained via dynamic diffraction by crystal slabs carved from a single Si monocrystal. Such monolithic interferometers were first demonstrated for x rays by Bonse and Hart [5] and subsequently for thermal neutrons by Rauch and collaborators [6].

The proof that neutron interference is possible using split-crystal interferometers [7] opens the way to extended arm separation and length and to experiments exploring quantum mechanics and gravity [8–12]. Realizing and using split-crystal interferometers requires mastering a detailed model of its operation. A subsequent paper will uses the formalism developed here to investigate numerically the contributions to the neutron phase of geometrical aberrations and dynamical diffraction [13].

The theoretical background is the dynamical scattering of neutrons by perfect crystals in the Earth's gravitational field. After its application to modeling the Colella-Overhauser-Werner experiments [2–4,14–17], discrepancies remain between the measured and predicted values of phase shift due to gravity. The measured values are lower than the theoretically predicted ones by about 1%, with relative uncertainties of about 0.1% [4,18,19]. Since there is no scientific basis for this difference, it must arise from a neglected effect in the interferometer operation.

Therefore, we reexamined the Laue diffraction of neutrons by perfect crystals and the operation of crystal interferometers, including geometrical aberrations and the gravitational and Coriolis forces by first principles.

Our approach is based on optical transfer matrices that map incoming into outgoing wave packets [20,21]. They accomplish the quantum-mechanical propagation of the neutron state—either pure or mixed—in free space and crystals. Hence, the interferometer is modeled by a sequence of propagations in crystals and free space that can be easily translated into a code for numerical or symbolic computations. Also, this approach allows aberration to be easily integrated into the model and their effects on the quantum-mechanical phase of the neutron to be quantified.

The paper is organized as follows: After introducing, in Sec. II, the neutron quantum states in the interferometer, in Sec. III, we give the analytical expression of the transfer matrix for their propagation in free space under the action of gravitational and Coriolis forces. Section IV copes with the Laue propagation in a perfect crystal, again under the action of Earth's gravity and rotation, and gives the closed-form expression of the relevant transfer matrix.

Section V concatenates free-space and crystal propagations to build the transfer matrix of the interferometer and discusses the effects of geometrical aberrations on the fringe phase. Sections V A and V B describe the interferometer operation based first on the excesses of accumulated phase due to the transferred momenta and next on the vantage point of the falling neutron. Section VI examines the interference signal.

Dynamical diffraction is a complex theory that requires abstruse calculations. Since they make it difficult to understand the underlying ideas and logic, we excluded most of them from the main paper, which only includes the starting

*Corresponding author: c.sasso@inrim.it
†Contact author: g.mana@inrim.it
‡Contact author: e.massa@inrim.it

points and results. We tried to discuss them in detail to help the understanding. Readers interested in using and verifying our results will find a report of the algebraic steps and analytical computations in the Supplemental Material [22]. Appendix F provides a list of the main symbols.

All the symbolic computations were carried out with the aid of *Mathematica* [23]; the relevant notebook is given as Supplemental Material [22]. To view and interact with it, download the Wolfram Player free of charge [24].

II. NEUTRON QUANTUM STATES IN THE INTERFEROMETER

Before discussing neutron propagation in free space and crystals, we introduce the reference frame and the notations we use to describe the neutron quantum state in the interferometer. We limit to plane-parallel crystals symmetrically cut, where the normal $\hat{\mathbf{z}}$ to the crystal surfaces is orthogonal to the reciprocal vector $\mathbf{h} = -2\pi\hat{\mathbf{x}}/d$ (d is the spacing of the diffracting planes). Jointly with the crystal vertical, $\hat{\mathbf{y}}$, $\hat{\mathbf{z}}$ and the horizontal axis, $\hat{\mathbf{x}} = -\hat{\mathbf{h}}$, define a right-handed coordinate system. The position vector $\mathbf{r} = (\mathfrak{r}, z)$ is split in the $\mathfrak{r} = (x, y)$ (lying in the crystal surface) and z components.

For each momentum state, two guided modes, which are superpositions of the transmitted, $|\Psi_o\rangle$, and diffracted, $|\Psi_h\rangle$, states, are excited within the crystal. Therefore, we describe each neutron, both in free space and in interferometer crystals, by the single-particle state $|\Psi\rangle = |\Psi_o\rangle + |\Psi_h\rangle$, where

$$\langle\mathbf{r}|\Psi\rangle = \psi_o(\mathfrak{r};z)\langle\mathbf{r}|o\rangle + \psi_h(\mathfrak{r};z)\langle\mathbf{r}|h\rangle, \tag{1a}$$

$$\langle\mathbf{r}|o\rangle = \mathrm{e}^{-\mathrm{i}\mathbf{K}_o\cdot\mathbf{r}}\mathrm{e}^{-\mathrm{i}K\chi_0 z/(2\gamma)}\begin{bmatrix}1\\0\end{bmatrix}, \tag{1b}$$

$$\langle\mathbf{r}|h\rangle = \mathrm{e}^{-\mathrm{i}\mathbf{K}_h\cdot\mathbf{r}}\mathrm{e}^{-\mathrm{i}K\chi_0 z/(2\gamma)}\begin{bmatrix}0\\1\end{bmatrix}, \tag{1c}$$

and

$$|\psi(\mathfrak{r};z)\rangle = \begin{bmatrix}\psi_o(\mathfrak{r};z)\\ \psi_h(\mathfrak{r};z)\end{bmatrix}. \tag{1d}$$

It belongs to the tensor product $L_2(\mathbb{R}^2)\otimes V_2$ of the $L_2(\mathbb{R}^2)$ space of the square-integrable two-variable functions and the two-dimensional vector space V_2 [20] and propagates along z, the optical axis, that plays the role of time.

The angular wave vectors [25]

$$\mathbf{K}_{o,h} = K[\pm\sin(\Theta_B)\hat{\mathbf{x}} + \cos(\Theta_B)\hat{\mathbf{z}}] \tag{2}$$

satisfy the Bragg conditions $\mathbf{K}_h = \mathbf{K}_o + \mathbf{h}$ and $|\mathbf{K}_o| = |\mathbf{K}_h| = K = mV/\hbar$, where Θ_B is the Bragg angle, $\hbar$ is the reduced Planck constant, and m and V the neutron mass and velocity, respectively. Also, we consider a coplanar geometry; that is, $\mathbf{K}_o$, $\mathbf{K}_h$, $\mathbf{h}$, and $\hat{\mathbf{z}}$ are in the same plane. In (2) and the following, the plus (minus) sign refers to the o (h) state.

We kept the effects of absorption, $\mu = \mathrm{Im}(\chi_0)K$, and refractive index, $n_0 - 1 = \mathrm{Re}(\chi_0)/2$, apart, in the $\exp[\mathrm{i}K\chi_0 z/(2\gamma)]$ factor, where $\gamma = \cos(\Theta_B)$, $\chi_0 = 0$ in a vacuum, and the sign $\mathrm{Im}(\chi_0)$ is that of the exponent of the plane waves. In our analysis, this factor is unessential and will be omitted.

The position and momentum representations, $\Psi_n(\mathbf{r})$ and $\widetilde{\Psi}_n(\mathbf{p})$, of the state $|\Psi_n\rangle$ are related by

$$\Psi_n(\mathbf{r}) = \frac{1}{(2\pi)^{3/2}}\int_{-\infty}^{+\infty}\widetilde{\psi}_n(\mathbf{p})\mathrm{e}^{-\mathrm{i}(\mathbf{K}_n+\mathbf{p})\cdot\mathbf{r}}\mathrm{d}\mathbf{p}, \tag{3a}$$

where $\hbar\mathbf{K}_n = m\mathbf{V}_n$ is the (mechanical and unperturbed) momentum, $\hbar\mathbf{p} = m\mathbf{v}$ is the momentum deviation from $\hbar\mathbf{K}_n$, $\mathbf{V}_n$, and $\mathbf{v}$ are the relevant velocities, and $n = o, h$. To avoid confusion with the reciprocal vector $\mathbf{h}$, we will always use the reduced Planck's constant $\hbar$. For the sake of simplicity, with somewhat incongruous terminology, we will indicate the angular wave vectors by their associated momenta, expressed in units of inverse length.

We are looking for quasi-plane waves propagating in the $\mathbf{K}_o$ and $\mathbf{K}_h$ directions. Their momentum representations have well-spaced peaks centered on $\mathbf{K}_o$ and $\mathbf{K}_h$ with negligible width. Therefore, $|\mathbf{p}| \ll K$. For the sake of simplicity, we also assume the expected value of $\mathbf{p}$ is null, that is, $\langle\mathbf{p}\rangle = (0, 0, 0)$.

Once the $\exp(\mathrm{i}\mathbf{K}_{o,h}\cdot\mathbf{r})$ plane waves are removed, the axis of propagation, denoted by z, plays the role of time (even though it's measured in space units) and the neutron lives in the xy plane. This implies that the z component of $\mathbf{p}$ represents an angular frequency measured in inverse space units.

By setting $\mathbf{p} = (\mathbf{q}, p_z)$ and $\mathbf{q} = (q_x, q_y)$, the partial Fourier transform of $\psi_n(\mathbf{r})$ is (see Appendix A)

$$\widetilde{\psi}_n(\mathbf{q};z) = \frac{1}{\sqrt{2\pi}}\int_{-\infty}^{+\infty}\widetilde{\psi}_n(\mathbf{p})\mathrm{e}^{-\mathrm{i}p_z z}\mathrm{d}p_z. \tag{3b}$$

We use the term resonance error to refer to the deviation $\mathbf{p}$ of a plane wave from perfect Bragg alignment. Moreover, when $\mathbf{p}$ is zero, the crystal resonates similarly to an optical cavity fed by a well-matched laser beam.

III. FREE FALL

Between the crystals that form the interferometer, neutrons travel through free space. Therefore, we need the transfer matrix that maps the neutron state at the crystal output surface to the state at the next crystal input surface.

We propagate the stationary states o and h along the optical axis z by the time-dependent Feynman propagator [26–28]. With a somewhat incongruous notation, we use the same symbol for the quantum-mechanical operator and the expected value of the associated quantity, understanding that it indicates the operator or the expected value depending on the context.

Without distinguishing between inertial and gravitational masses, the Hamiltonian for a neutron in a uniform gravitational field and Earth's rotating frame is [4,29,30]

$$H_n = \frac{\hbar^2 k_n^2}{2m} - m\mathbf{g}\cdot\mathbf{r} - \hbar(\Omega\mathbf{r})\cdot\mathbf{k}_n, \tag{4}$$

where $\mathbf{k}_n = \mathbf{K}_n + \mathbf{p}$ is the wave vector of the $\mathbf{q}$ mode $\psi_n(\mathfrak{r};z) = \exp(-\mathrm{i}\mathbf{p}\cdot\mathbf{r})$, $n = o, h$, $\mathbf{r}$ is the local neutron's position,

$$\mathbf{g} = -\frac{GM_\oplus}{R_\oplus^2}\hat{\mathbf{R}}_\oplus - \boldsymbol{\omega}\times(\boldsymbol{\omega}\times\mathbf{R}_\oplus)$$

is the acceleration due to gravity and the centrifugal force, $\boldsymbol{\omega}$ is the Earth's angular velocity, and $\mathbf{R}_\oplus$ is taken from the center of the Earth to the origin of the local reference frame.

Since, in a right-handed reference frame, the operator $\boldsymbol{\omega}\times$ can be represented by the antisymmetric matrix

$$\Omega = \begin{bmatrix} 0 & -\omega_z & \omega_y \\ \omega_z & 0 & -\omega_x \\ -\omega_y & \omega_x & 0 \end{bmatrix}$$

in (4), we wrote $\boldsymbol{\omega} \times \mathbf{r}$ as $\Omega\mathbf{r}$. For the sake of simplicity, we omit the subscript $n = o, h$ in the position vector $\mathbf{r}$, velocity perturbation $\mathbf{v}$, and resonance error $\mathbf{p}$. The last two depend on n because of the different Coriolis forces acting on the o and h states.

The canonical momentum $\hbar\mathbf{k}_n = \hbar(\mathbf{K}_n + \mathbf{p})$ is the variable conjugate to $\mathbf{r}$. Therefore, the Fourier dual of $\mathbf{r}$, which is $\mathbf{p}$, is related to the kinetic momentum $m\mathbf{v}$ by $\hbar\mathbf{p} = m(\mathbf{v} + \Omega\mathbf{r})$ [4].

Starting from (4) and (3a), the time-independent Schrödinger equation is

$$\left(\frac{\hbar^2 k_n^2}{2m} - m\mathbf{g}\cdot\mathbf{r} + 2\hbar(\Omega\mathbf{K}_n)\cdot\mathbf{r}\right)\widetilde{\psi}_n(\mathbf{p}) = \frac{\hbar^2 K^2}{2m}\widetilde{\psi}_n(\mathbf{p}), \quad (5)$$

where $\hbar^2K^2 = 2mE$ and E is the energy. On condition that $p \ll K_z$, we made the approximation

$$\begin{aligned}(\Omega\mathbf{r})\cdot(\mathbf{K}_n + \mathbf{p}) &\approx \mathbf{K}_n\cdot(\Omega\mathbf{r}) + \frac{z}{K_z}(\Omega\mathbf{K}_n)\cdot\mathbf{p} \\ &\approx -(\Omega\mathbf{K}_n)\cdot\mathbf{r}, \end{aligned} \quad (6)$$

where we replaced $\mathbf{r}$ with $z\mathbf{K}_n/K_z$, which is the unperturbed trajectory of the $n = o, h$ state, see Appendix C. This approximation also requires that the trajectory perturbations due to gravity and Coriolis force are small (relative to z/γ). Eventually, the left- and right-multiplication of the matrix $\boldsymbol{\Omega}$ and the wave vector $\mathbf{K}_n$ are related by $\mathbf{K}_n\Omega = \Omega^T\mathbf{K}_n = -\Omega\mathbf{K}_n$.

As shown in Appendixes D 1 and D 2, the term $(\Omega\mathbf{r})\cdot\mathbf{p}$ omitted in (6) encodes the $m(\Omega\mathbf{r})$ difference between the canonical, $\hbar\mathbf{p}$, and kinematical, $m\mathbf{v}$, momenta. Since the potential term of the approximate Hamiltonian in (5) does not depend on the velocity perturbation $\mathbf{v}$, the canonical and kinematical momenta must be the same, i.e., $\hbar\mathbf{p} = m\mathbf{v}$. The factor of two multiplying $(\Omega\mathbf{K}_n)\cdot\mathbf{r}$ in (5)—which is not present in (6)—ensures the fulfillment of this requirement, see Appendix D 2. Besides, the potential of the approximated Coriolis force $-2\hbar(\Omega\mathbf{K}_n)$ is $2\hbar(\Omega\mathbf{K}_n)\cdot\mathbf{r}$, not $(\Omega\mathbf{K}_n)\cdot\mathbf{r}$.

Since the approximate force $-2\hbar(\Omega\mathbf{K}_n)$ in (5) is a constant, we can pool it with the gravitational force $m\mathbf{g}$, define the total force acting on the $n = o, h$ neutron state as, see Appendix B,

$$\mathbf{f}_n = (f_x, f_{ny}.f_{nz})^T = \frac{m}{\hbar^2 K_z}[m\mathbf{g} - 2\hbar(\Omega\mathbf{K}_n)], \quad (7)$$

and rewrite (5) accordingly.

Given the state $|\widetilde{\psi}(\mathbf{q}';0)\rangle$ at the input plane $z = 0$ and assuming the separation of the q_x and q_y variables, the solution of the Schrödinger equation (5), see Ref. [22], is

$$\begin{aligned}|\widetilde{\psi}(\mathbf{q};z)\rangle = &\begin{bmatrix} \exp(-\mathrm{i}K_z\delta_o z) & 0 \\ 0 & \exp(-\mathrm{i}K_z\delta_h z) \end{bmatrix} \\ &\times \int_{-\infty}^{+\infty} \widetilde{F}(\mathbf{q},\mathbf{q}';z)|\widetilde{\psi}(\mathbf{q}';0)\rangle \mathrm{d}\mathbf{q}', \end{aligned} \quad (8a)$$

where the $\widetilde{F}(\mathbf{q},\mathbf{q}';z) = \widetilde{F}_x(q_x,q_x';z)\widetilde{F}_y(q_y,q_y';z)$ factors are

$$\begin{aligned}\widetilde{F}_x(q_x,q_x';z) = &\exp\left(\frac{\mathrm{i}q_x^2 z}{2K_z} + \frac{\mathrm{i}\delta q_x\delta x}{3} - \mathrm{i}q_x\delta x\right)\delta(q_x' - q_x + f_x z) \\ &\times \begin{bmatrix} \exp\left[+\mathrm{i}(q_x z\tan(\Theta_B) - K_x\delta x)\right] & 0 \\ 0 & \exp[-\mathrm{i}(q_x z\tan(\Theta_B) - K_x\delta x)] \end{bmatrix}, \end{aligned} \quad (8b)$$

$$\widetilde{F}_y(q_y,q_y';z) = \begin{bmatrix} \exp\left(\frac{\mathrm{i}q_y^2 z}{2K_z} + \frac{\mathrm{i}\delta_o q_y\delta_o y}{3} - \mathrm{i}q_y\delta_o y\right)\delta(q_y' - q_y + f_{oy}z) & 0 \\ 0 & \exp\left(\frac{\mathrm{i}q_y^2 z}{2K_z} + \frac{\mathrm{i}\delta_h q_y\delta_h y}{3} - \mathrm{i}q_y\delta_h y\right)\delta(q_y' - q_y + f_{hy}z) \end{bmatrix}. \quad (8c)$$

This transfer matrix propagates the neutron state through the spaces between the interferometer crystals. In the Appendixes C and D, we verify its derivation by comparing its internal logic with the unperturbed and perturbed quantum trajectories of the neutron. The following paragraphs explain the origin and significance of the quantities that define $\widetilde{F}(\mathbf{q},\mathbf{q}';z)$.

First, if $\mathbf{f}_n = (0,0,0)^T$, $\widetilde{F}(\mathbf{q},\mathbf{q}';z)$ reduces to the free-space propagator. Next, the Dirac's deltas indicate that the final $\mathbf{p}$ mode leaves the initial $z = 0$ plane as $\mathbf{p}' = \mathbf{p} - \delta_n\mathbf{p}$, where $\hbar\delta_n\mathbf{p} = \hbar(\delta_n\mathbf{q}, f_{nz}z)$ is the momentum transferred by the pooled forces ($m\mathbf{g}$ and $-2m\Omega\mathbf{V}_n = -2\hbar\Omega\mathbf{K}_n$) acting for the time interval $mz/(\hbar K_z)$, see Appendix D. The $\delta_n\mathbf{p}$ components are

$$\begin{aligned}\delta q_x &= f_x z = \frac{m^2 g_x z}{\hbar^2 K_z} - \frac{2m\omega_y z}{\hbar}, \\ \delta_n q_y &= f_{ny} z = \frac{m^2 g_y z}{\hbar^2 K_z} + \frac{2m[\omega_x \pm \omega_z\tan(\Theta_B)]z}{\hbar}, \\ \delta_n p_z &= f_{nz} z = \frac{m^2 g_z z}{\hbar^2 K_z} \mp \frac{2m\omega_y\tan(\Theta_B)z}{\hbar}. \end{aligned} \quad (9a)$$

From the shift property of the Fourier transform, we see that

$$\begin{aligned}\delta x &= \frac{f_x z^2}{2K_z} = \frac{m^2 g_x z^2}{2\hbar^2 K_z^2} - \frac{m\omega_y z^2}{\hbar K_z},\\ \delta_n y &= \frac{f_{ny} z^2}{2K_z} = \frac{m^2 g_y z^2}{2\hbar^2 K_z^2} + \frac{m[\omega_x \pm \omega_z \tan(\Theta_B)]z^2}{\hbar K_z},\\ \delta_n z &= \frac{f_{nz} z^2}{2K_z} = \frac{m^2 g_z z^2}{2\hbar^2 K_z^2} \mp \frac{m\omega_y \tan(\Theta_B) z^2}{\hbar K_z}\end{aligned} \tag{9b}$$

are the components of the trajectory perturbation $\delta_n \mathbf{r} = (\delta_n \mathfrak{x}, \delta_n z)$ due to the pooled forces, $m\mathbf{g}$ and $-2\hbar\Omega\mathbf{K}_n$ acting for the $mz/(\hbar K_z)$ time interval.

The unperturbed trajectories fulfilling the Bragg conditions (identified by the $\mathbf{q} = 0$ modes, which will be termed base rays) are the straight lines where $x_{o,h} = \pm z \tan(\Theta_B)$ and $y = 0$. Therefore, it follows that excess phases

$$\begin{aligned}\int_0^z f_x z \mathrm{d}x_{o,h} &= \pm f_x z^2 \tan(\Theta_B)/2 = \pm K_x \delta x,\\ \int_0^z f_{ny} z \mathrm{d}y &= 0,\\ \int_0^z f_{nz} z \mathrm{d}z &= f_{nz} z^2/2 = K_z \delta_n z\end{aligned} \tag{9c}$$

can be understood by integrating the (transversal and longitudinal) transferred momenta over the unperturbed trajectory.

Since

$$\begin{aligned}\frac{1}{2K_z}\int_0^z (q_x - f_x z)^2 \mathrm{d}z &= \frac{q_x^2 z}{2K_z} + \frac{f_x^2 z^3}{6K_z} - q_x \delta x\\ &= \frac{q_x^2 z}{2K_z} + \frac{\delta q_x \delta x}{3} - q_x \delta x,\end{aligned} \tag{9d}$$

the phases in the exponential factor of $\widetilde{F}_x(q_x, q'_x; z)$ and $\widetilde{F}_y(q_y, q'_y; z)$, account for diffraction and are related to the change of $\mathbf{q}$ along the unperturbed trajectories.

IV. LAUE DIFFRACTION

The last thing we need is the transfer matrix that maps the neutron state at the input surface of the interferometer crystals to the one at the output surface.

In the presence of gravitational and Coriolis forces, the neutron wave function in a crystal complies with the time-independent Schrödinger equation [31],

$$\begin{aligned}&\left[-\frac{\hbar^2\Delta}{2m} + \frac{\hbar^2 K^2 \chi(\mathbf{r})}{2m} - m\mathbf{g}\cdot\mathbf{r} - \mathrm{i}\hbar(\Omega\mathbf{r})\cdot\boldsymbol{\nabla}\right]\Psi'(\mathbf{r})\\ &\quad = \frac{\hbar^2 K^2}{2m}\Psi'(\mathbf{r}),\end{aligned} \tag{10a}$$

where

$$\begin{aligned}\Psi'(\mathbf{r}) &= \Psi_o(\mathbf{r}) + \Psi_h(\mathbf{r})\\ &= [\psi_o(\mathbf{r})\mathrm{e}^{-\mathrm{i}\mathbf{K}_o\cdot\mathbf{r}} + \psi_h(\mathbf{r})\mathrm{e}^{-\mathrm{i}\mathbf{K}_k\cdot\mathbf{r}}]\mathrm{e}^{-\mathrm{i}K\chi_0 z/(2\gamma)},\end{aligned} \tag{10b}$$

and

$$\chi(\mathbf{r}) = \sum_{\mathbf{h}\neq 0} \chi_h \mathrm{e}^{-\mathrm{i}\mathbf{h}\cdot\mathbf{r}} \tag{10c}$$

is the dimensionless Fermi pseudopotential of the crystal. The χ_0 term is excluded from the Fourier expansion because we already factored it in $\Psi'(\mathbf{r})$. To keep compliance with the dynamical theory formalism, the dimensionless coefficients of the Fourier expansion of $\chi(\mathbf{r})$ are redefined as [18]

$$\chi_h = \frac{4\pi b}{K^2 V_{\mathrm{cell}}} \sum_j \mathrm{e}^{-\mathrm{i}\mathbf{h}\cdot\mathbf{r}_j},$$

where b is the neutron (coherent) scattering length of the Si nucleus and j labels the Si atoms in the (cubic) unit cell. The $\chi_{\pm h}$ phases depend on the origin of the reference frame; a translation $\mathbf{u}$ changes $\chi_{\pm h}$ according to $\chi_{\pm h} \to \chi_{\pm h}\exp(\pm\mathrm{i}\mathbf{h}\cdot\mathbf{u})$. We assume that $\chi(-x, y; z) = \chi(x, y; z)$, so that $\chi_h = \chi_{-h}$. Since $\exp(\pm\mathrm{i}\pi) = -1$, the sign of $\chi_{\pm h}$ can be chosen either positive or negative.

Equation (10a) is the equivalent of (5), where, in addition to the pooled forces, we took the interaction with the crystal into account. Assuming a symmetrically cut (plane-parallel) crystal slab, Fourier transforming (10a), using (3a), applying the differentiation and convolution properties of the transform, and neglecting second-order terms proportional to $(p/K_z)^2$, we obtain the Takagi-Taupin equations

$$\begin{bmatrix} -D_{oz} & 0\\ 0 & -D_{hz}\end{bmatrix}\begin{bmatrix}\widetilde{\psi}_o(\mathbf{q}; z)\\ \widetilde{\psi}_h(\mathbf{q}; z)\end{bmatrix} = \begin{bmatrix} q_x\tan(\Theta_B) + \mathrm{i}f_x\partial_{q_x} + \mathrm{i}f_{oy}\partial_{q_y} & -\upsilon\\ -\upsilon & -q_x\tan(\Theta_B) + \mathrm{i}f_x\partial_{q_x} + \mathrm{i}f_{hy}\partial_{q_y}\end{bmatrix}\begin{bmatrix}\widetilde{\psi}_o(\mathbf{q}; z)\\ \widetilde{\psi}_h(\mathbf{q}; z)\end{bmatrix}, \tag{11}$$

where $D_{nz} = \mathrm{i}\partial_z - f_{nz} z$ and $\upsilon = \chi_{+h}K/(2\gamma) = \chi_{-h}K/(2\gamma)$. Details about the Fourier-optics approach to the dynamical theory of x-ray and neutron diffraction in crystals and the derivation of (11) are given in Refs. [20,32].

We found the transfer matrix $U(t)$ for the propagation of the quantum state $|\widetilde{\psi}(\mathbf{q}'; 0)\rangle$ given at the input surface $z = 0$ trough a crystal slab having thickness t by solving the Takagi-Taupin equations (11), see Ref. [22]. The solution is

$$|\widetilde{\psi}(\mathbf{q}; t)\rangle = \int_{-\infty}^{+\infty} \widetilde{U}(\mathbf{q}, \mathbf{q}'; t)|\widetilde{\psi}(\mathbf{q}'; 0)\rangle \mathrm{d}\mathbf{q}', \tag{12a}$$

where

$$\widetilde{U}(\mathbf{q},\mathbf{q}';t)=\delta(q'_x-q_x+f_xt)\exp\left(\frac{\mathrm{i}q^2t}{2K_z}-\mathrm{i}K_z\delta t\right)\begin{bmatrix} T(q_x-f_xt/2;t) & \exp(-\mathrm{i}h\bar{u})R(q_x-f_xt/2;t) \\ \times\delta(q'_y-q_y+f_{oy}t) & \times\delta(q'_y-q_y+f_yt) \\ \exp(+\mathrm{i}h\bar{u})R(q_x-f_xt/2;t) & T(-q_x+f_xt/2;t) \\ \times\delta(q'_y-q_y+f_yt) & \times\delta(q'_y-q_y+f_{hy}t) \end{bmatrix}. \tag{12b}$$

For the definitions of the symbols used refer also to Appendix F and Figs. 1 and 2. In the following, we detail the origin and meaning of the quantities that determine $\widetilde{U}(\mathbf{q},\mathbf{q}';t)$ and its internal logic.

The functions

$$R(q;t)=-\frac{\mathrm{i}\sin\left(\Delta f_zt^2/2+\zeta\sqrt{\eta^2+1}\right)}{\sqrt{\eta^2+1}}, \tag{13a}$$

$$T(q;t)=\cos\left(\Delta f_zt^2/2+\zeta\sqrt{\eta^2+1}\right)-\eta R(\eta;\zeta), \tag{13b}$$

where $\zeta=\pi t/\Lambda_e$, $\eta=\Lambda_e\tan(\Theta_B)q/\pi$, and $\Lambda_e=\lambda\gamma/|\chi_h|$ are the dimensionless thickness and resonance error and the *Pendellösung* length, respectively, are the (amplitude) reflection and transmission coefficients, in Laue geometry, of the crystal slab. They summarize the propagation given by Horne [16] and Littrell [33] in terms of mode matching and dispersion surface. The limits as $\chi_h\to 0$ and $|\eta|\to\infty$ duplicate the first-order approximation of the free-space propagation (8a)–(8c), refer to Ref. [24] for the proof.

The $\exp(\mp\mathrm{i}h\bar{u})$ factors of the off-diagonal terms show that propagation occurs in the same way as in a deformed crystal [32,34], where the diffracting planes are shifted along the horizontal axis in the direction opposite to half of the total displacement of the neutron in the crystal,

$$\bar{u}=-\frac{f_xt^2}{K_z}=-\frac{\delta x(t)}{2}. \tag{14a}$$

The argument of the transmission and reflection coefficients show that the neutron sees the diffracting planes rotated about

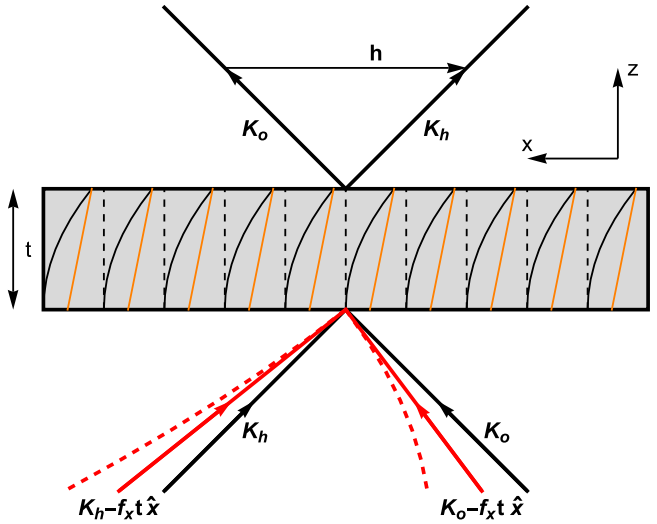

FIG. 1. Gravitational and Coriolis forces in neutron Laue diffraction. The neutron falls in the positive x direction. Black dashed lines show diffracting planes. Solid lines show perceived deformed planes (black) and effectively tilted and displaced planes (red). $\mathbf{h}$ is the reciprocal vector, $\mathbf{K}_{o,h}$ are wave vectors satisfying the Bragg law. Black rays show plane waves propagating in the $\mathbf{K}_{o,h}$ directions. Red lines show neutron trajectory (dashed) and incoming rays leaving the crystal in the $\mathbf{K}_{o,h}$ directions (solid). The transferred momentum $f_xt\hat{\mathbf{x}}$ makes $\mathbf{K}_{o,h}-f_xt\hat{\mathbf{x}}$ satisfy the Bragg condition for the tilted planes (red). t is the crystal thickness

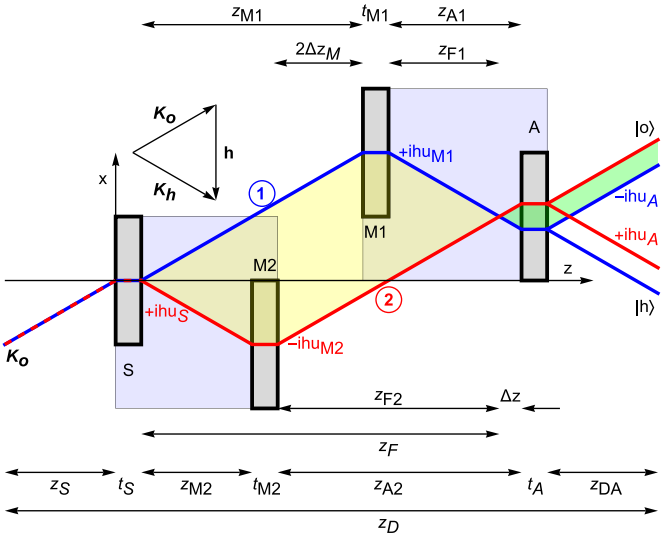

FIG. 2. Skew-symmetric LLL interferometer with separate crystals (crystal top-view). S is a splitter, M1 and M2 are mirrors, and A is an analyzer. The blue and red base rays (the unperturbed trajectories fulfilling the Bragg condition $\mathbf{q}=0$) indicate the 1st and 2nd arms, respectively. The horizontal x axis is orthogonal to the diffracting planes. The crystal vertical y points up. The optical axis z is normal to the crystals' surfaces. The input state is labeled o. z_S and z_{DA} are the source and detector distances from the splitter and analyzer, respectively. The gaps between the ith mirror and the splitter and analyzer are z_{Mi} and z_{Ai}, respectively. The skewness $2\Delta_M=z_{M2}-z_{M1}$ is the mirrors' gap. The split rays are recombined in the interferometer focal plane, which, in the absence of geometric aberrations, is the analyzer input surface. z_{F1} and z_{F2} are the focal-plane distance from the mirrors; z_F is the distance of the splitter from the focal plane (or, without geometrical aberration, from the analyzer). The $\pm\mathrm{i}hu$ labels are the phases gained by the reflected state relative to the forward-transmitted one.

the vertical by

$$\theta = -\frac{f_x t}{2K_z}, \tag{14b}$$

which is opposite to the mean change of its propagation direction in the crystal.

The z components of the Coriolis forces acting on the h and o states are different, resulting in different axial momenta transferred to the neutron. The $2\Delta f_z = f_{hz} - f_{oz}$ difference originates the $\Delta f_z t^2/2$ offset of the arguments of the transmission and reflection coefficients and makes the effective crystal-thickness different from the geometrical one. This difference was not spotted in previous investigations [3,15–17].

The shared phase $K_z\delta t$, where $\delta t = (\delta_o t + \delta_h t)/2$ is the (mean) difference between the perceived and actual thickness, originates from the axial moment $(\delta p_z)t$, where $\delta p_z = (\delta_o p_z + \delta_h p_z)/2$. We heuristically added the $q^2 t/(2K_z)$ shared phase, because it rules the horizontal and vertical shears of the interfering beams (see also Appendix D 4).

As in free space, the Dirac deltas account for the vertical $f_{ny}t$ and $f_y t$ and horizontal $f_x t$ momentum transfers, where $f_y = (f_{hy} + f_{oy})/2$ is the mean of the vertical components of the pooling of gravity and Coriolis force.

In (8b) and (8c), the $q_x\delta x$ and $q_y\delta_n y$ phases encode the neutrons falls along the x and y axes. They are second-order effects originated by the wave-function diffraction, see (9d). On the contrary, the phases of the $\widetilde{U}(\mathbf{q}, \mathbf{q}'; t)$ elements do not depend linearly on q_x and q_y. This means that, in crystals, neutrons propagate parallel to the z axis. As shown by the unperturbed and perturbed quantum trajectories of the neutron given in the Appendixes C 2 and D 4, provided $\langle \mathbf{q} \rangle = (0, 0)^T$, the Takagi-Taupin equations (11) implies that neutrons are guided along the diffracting planes, regardless of gravity and Coriolis force. However, this is not a characteristic of guided propagation in crystals but rather a consequence of the Takagi-Taupin equations omitting the second-order terms.

Omitting the shared factor $\exp(-\mathrm{i}K_z\delta t)$, which is due to the longitudinal acceleration, the waves leaving a plane-parallel crystal symmetrically cut are (see Ref. [24] and Fig. 1)

$$\widetilde{\psi}_{oo}(\mathbf{q}; t) = T(q_x - f_x t/2; t)\widetilde{\psi}_o(q_x - f_x t, q_y - f_{oy}t; 0), \tag{15a}$$

$$\widetilde{\psi}_{ho}(\mathbf{q}; t) = R(q_x - f_x t/2; t)\widetilde{\psi}_o(q_x - f_x t, q_y - f_y t; 0) \times \exp(+\mathrm{i}h\overline{u}) \tag{15b}$$

if the initial state is $|\widetilde{\psi}(\mathbf{q}; 0)\rangle = \widetilde{\psi}_o(\mathbf{q}; 0)|o\rangle$, and

$$\widetilde{\psi}_{hh}(\mathbf{q}; t) = T(-q_x + f_x t/2; t)\widetilde{\psi}_h(q_x - f_x t, q_y - f_{hy}t; 0), \tag{15c}$$

$$\widetilde{\psi}_{oh}(\mathbf{q}; t) = R(q_x - f_x t/2; t)\widetilde{\psi}_h(q_x - f_x t, q_y - f_y t; 0) \times \exp(-\mathrm{i}h\overline{u}) \tag{15d}$$

if the initial state is $|\widetilde{\psi}(\mathbf{q}; 0)\rangle = \widetilde{\psi}_h(\mathbf{q}; 0)|h\rangle$.

The neutron sees a displacement of the diffracting planes opposite to half its fall while crossing the crystal. Consequently, the phase of the reflected wave is changed by $\pm h\overline{u}$ relative to the forward-transmitted one. With the adopted sign conventions, a wave propagating in the positive x direction accumulates a negative phase. Therefore, in absolute terms, the phase is decreased if the displacement $\overline{u}$ has the same direction as the incoming wave, see (15b), and increased otherwise, see (15d).

The leaving $\mathbf{q}$ mode enters the crystal as the $\mathbf{q} - (f_x\hat{\mathbf{x}} + f_{ny}\hat{\mathbf{y}})t$ mode. This means that the pooled forces transfer the $\hbar(f_x\hat{\mathbf{x}} + f_{ny}\hat{\mathbf{y}})t$ momentum. No phase proportional to q_x and q_y appears in the equations (15). This confirms that the neutrons propagate in a straight line and that the Takagi-Taupin equations fail to capture their fall. Eventually, it is worth noting that the crystal reflection is never specular, also if $\mathbf{f}_n = \mathbf{0}$ and in the limit as the crystal thickness tends to zero [35].

V. CRYSTAL INTERFEROMETRY

Eventually, we build the transfer matrix for the neutron propagation from the source to the detector by multiplying the matrices relevant to propagation in the free spaces and crystals.

Owing to the limited spatial coherence of the sources, that is, the limited capacity to prepare every neutron in the same state, we should consider a probabilistic superposition of single-particle wave packets. Assuming a Gaussian Shell model of the superposition, the integrated densities are the same as those yielded by a coherent Gaussian source, having a radius equal to the coherence length [36,37]. Therefore, we simplify the following algebra by limiting the analysis to this coherent source.

As shown in Fig. 2, a shew-symmetric triple-Laue interferometer consists of four plane parallel (symmetrically cut) crystals that split and recombine the neutron wave function via consecutive diffractions and create a Mach-Zehnder interferometer. The propagation through the interferometer is given by

$$|\psi_{\mathrm{out}}\rangle = [X_1 + X_2]|\psi_{\mathrm{in}}\rangle, \tag{16a}$$

where we omit to indicate the source and detector z coordinates, which are implied in the in and out subscripts, and

$$X_1 = F(z_{DA})U(t_A)F(z_{A1})P_h U(t_{\mathrm{M1}})F(z_{\mathrm{M1}})P_o U(t_S)F(z_S), \tag{16b}$$

$$X_2 = F(z_{DA})U(t_A)F(z_{A2})P_o U(t_{\mathrm{M2}})F(z_{\mathrm{M2}})P_h U(t_S)F(z_S), \tag{16c}$$

propagate $|\psi_{\mathrm{in}}\rangle$ along the $i = 1, 2$ arms. The symbols for the thickness and spacing of the crystals have the meaning given in Fig. 2 and $P_n = |n\rangle\langle n|$ projects into the $|n\rangle$ state. The free-space transfer matrices used in (16b)–(16c) are obtained by approximating up to the first-order (8b) and (8c).

Hence,

$$\widetilde{F}(\mathbf{q},\mathbf{q}';z)=\begin{bmatrix}\exp\left[\mathrm{i}\left(q_x-\frac{f_xz}{2}\right)z\tan(\Theta_B)-\mathrm{i}K_z\delta_oz\right]\\ \times\delta\left(q'_y-q_y+f_{oy}z\right)\\ 0\end{bmatrix}\begin{matrix}0\\ \exp\left[-\mathrm{i}\left(q_x-\frac{f_xz}{2}\right)z\tan(\Theta_B)-\mathrm{i}K_z\delta_hz\right]\\ \times\delta\left(q'_y-q_y+f_{hy}z\right)\end{matrix}\times\ \delta(q'_x-q_x+f_xz)\exp\left(\frac{\mathrm{i}q^2z}{2K_z}\right). \tag{17}$$

We kept the overall phase proportional to $q^2=q_x^2+q_y^2$ because it rules the horizontal and vertical shears of the beams leaving the interferometer.

Since the momentum representations of $U(z)$ and $F(z)$ are not diagonal, assuming, without loss of generality, $|\psi_{\rm in}(\mathbf{q})\rangle=\widetilde{\psi}_{\rm in}(\mathbf{q})|o\rangle$, propagation

$$\begin{bmatrix}\widetilde{\psi}_{o1}(\mathbf{q})+\widetilde{\psi}_{o2}(\mathbf{q})\\ \widetilde{\psi}_{h1}(\mathbf{q})+\widetilde{\psi}_{h2}(\mathbf{q})\end{bmatrix}=\int_{-\infty}^{+\infty}[X_1(\mathbf{q},\mathbf{q}')+X_2(\mathbf{q},\mathbf{q}')]\begin{bmatrix}\widetilde{\psi}_{\rm in}(\mathbf{q}')\\ 0\end{bmatrix}\mathrm{d}\mathbf{q}' \tag{18}$$

requires an integration. The elements of the 2×2 matrices $X_1(\mathbf{q},\mathbf{q}')$ and $X_2(\mathbf{q},\mathbf{q}')$ are separable. Therefore, the integrations over q'_x and q'_y factorize and, omitting shared phases and second-order terms, the propagated waves are (refer to Ref. [24] for the calculations)

$$\widetilde{\psi}_{o1}(\mathbf{q})=R(q_x-q_{xA};t_A)R(q_x-q_{x1};t_{\rm M1})T(q_x-q_{xS};t_S)\widetilde{\psi}_{\rm in}(q_x-q_{x0},q_y-q_{yo}), \tag{19a}$$

$$\widetilde{\psi}_{o2}(\mathbf{q})=T(q_x-q_{xA};t_A)R(q_x-q_{x2};t_{\rm M2})R(q_x-q_{xS};t_S)\widetilde{\psi}_{\rm in}(q_x-q_{x0},q_y-q_{yo})\times\exp[\mathrm{i}(f_x\mathcal{A}_0+f_x\mathcal{A}_1+h\Delta u+q_x\Delta x+q_y\Delta y+\beta)], \tag{19b}$$

$$\widetilde{\psi}_{h1}(\mathbf{q})=T(-q_x+q_{xA};t_A)R(q_x-q_{x1};t_{\rm M1})T(q_x-q_{xS};t_S)\widetilde{\psi}_{\rm in}(q_x-q_{x0},q_y-q_{yh}), \tag{19c}$$

$$\widetilde{\psi}_{h2}(\mathbf{q})=R(q_x-q_{xA};t_A)R(q_x-q_{x2};t_{\rm M2})R(q_x-q_{xS};t_S)\widetilde{\psi}_{\rm in}(q_x-q_{x0},q_y-q_{yh})\times\exp[\mathrm{i}(f_x\mathcal{A}_0+f_x\mathcal{A}_1+h\Delta u+q_x\Delta x+q_y\Delta y+\beta)]. \tag{19d}$$

In Eqs. (19),

$$\begin{aligned}q_{x0}&=f_xz_D,\\ q_{xS}&=q_{x0}-f_x(z_S+t_S/2),\\ q_{xi}&=q_{xS}-f_x(t_S/2+z_{Mi}+t_{Mi}/2),\\ q_{xA}&=q_{xi}-f_x(t_{Mi}/2+z_{Ai}+t_A/2),\end{aligned} \tag{20a}$$

and

$$\begin{aligned}q_{yo}&=f_yz_D-\Delta f_y(z_S-2\Delta_M+z_{DA}+t_A),\\ q_{yh}&=f_yz_D-\Delta f_y(z_S-2\Delta_M-z_{DA})\end{aligned} \tag{20b}$$

are transferred momenta, $2\Delta_M=z_{\rm M2}-z_{\rm M1}$ is the interferometer skewness (the mirrors' gap), and z_D is the detector distance from the source.

The q_{x0} and q_{yn} offsets in the argument of the initial wave function encode the deflection at the source of the interfering $\mathbf{q}$ modes. They are nullified by the momentum transferred by the pooled forces in the propagation through the interferometer. The q_y offset depends on the $n=o,h$ state because of the different Coriolis forces acting on the neutron in the o or h state. Since the interfering $\mathbf{q}$ modes leave the source in the same mode, identified by $\mathbf{q}-q_{x0}\hat{\mathbf{x}}-q_{yn}\hat{\mathbf{y}}$, the partial coherence of the source does not cause visibility loss.

The effect of the pooled forces on the crystals' transmission and reflection is the same as a deviation from the exact Bragg's angle, which deviation depends on the crystal separations and is coded by the q_{xj} offsets of the arguments of the reflection and transmission coefficients ($j=S,1,2,A$ indicates the splitter, mirrors, and analyzer, respectively).

The q_{xS} offset, indicating the misalignment of the whole interferometer, is irrelevant and can be set to zero. The significant misalignments are those between the splitting and recombining lattice planes, which are pointed out by $q_{xA}-q_{xS}$ and $q_{xi}-q_{xS}$.

Five terms contribute to the difference between the phases accumulated in the interferometer arms. In the following, we discuss their origin, meaning, and internal logic.

The first term, $f_x\mathcal{A}_0$, is proportional to the area $\mathcal{A}_0$ enclosed by the base rays (the unperturbed rays fulfilling the Bragg conditions and corresponding to the $\mathbf{q}=0$ modes) [4]. This area, which is filled in yellow in Fig. 2, is given by

$$\mathcal{A}_0=2(t_Mz_M+z_{\rm M1}z_{\rm M2}-\Delta_{21}\Delta_M)\tan(\Theta_B), \tag{21}$$

where $t_M=(t_{\rm M1}+t_{\rm M2})/2$ and $z_M=(z_{\rm M1}+z_{\rm M2})/2$ are the mean mirrors' thickness and distance from the splitter, respectively, and $2\Delta_{21}=t_{\rm M2}-t_{\rm M1}$ and $2\Delta_M=z_{\rm M2}-z_{\rm M1}$ are the thickness difference and gap between the two mirrors,

respectively. The term

$$f_x\mathcal{A}_0 = \frac{m^2 g_x \mathcal{A}_0}{\hbar^2 K_z} - \frac{2m\omega_y \mathcal{A}_0}{\hbar} \tag{22}$$

includes the phase differences induced by gravity and Coriolis force, the last one being analogous to the Sagnac phase shift in optics [3,33].

When $f_x < 0$, the momentum of the neutron on the first arm is lower than that on the second one, see Fig. 2. This results in fewer phase accumulation in the first arm than in the second and in the expectation of a positive phase difference. The seeming contradiction with the negative sign of $f_x\mathcal{A}_0$, is solved by observing that, because of our conventional choices, the sign of the accumulated phase is negative, see (1a).

To compare our result with the usual expressions of the gravitationally induced phase difference, we note that, in Refs. [2,19,33], g_x/K_z is written as $g\sin\alpha/(K\cos\theta_B)$, where α is the (clockwise) rotation of the interferometer about the (leveled) incoming beam.

The second term, $f_x\mathcal{A}_1$, takes into account the interferometer defocus (a z translation of the analyzer away from the point where the interferometer arms are recombined)

$$\Delta z = z_{A1} - z_{M2} - \Delta_{21} = z_{A2} - z_{M1} + \Delta_{21}. \tag{23a}$$

It is proportional to the area

$$\mathcal{A}_1 = -2(t_A + z_{DA})\Delta z \tan(\Theta_B), \tag{23b}$$

which is filled in green in Fig. 2 and enclosed by the paths of the base rays from the focal plane to the detector. The $\mathcal{A}_1$ sign opposes the $\mathcal{A}_0$ sign because, with a positive defocus, the loop whereby the recombined neutron returns to the focus after reaching the detector is traveled oppositely to the $\mathcal{A}_0$ one. Unless the detector distance is large, it is a second-order term and can be neglected.

The term

$$\begin{aligned}\Delta u &= \bar{u}_S + \bar{u}_A - \bar{u}_{M1} - \bar{u}_{M2} \\ &= -\frac{f_x\left(t_S^2 + t_A^2 - t_{M1}^2 - t_{M2}^2\right)\tan(\Theta_B)}{2h},\end{aligned} \tag{23c}$$

which nullifies when $t_A = t_S = t_{M1} = t_{M2}$, takes the differences between the perceived crystals' deformations into account.

The fourth and fifth terms $q_x\Delta x$ and $q_y\Delta y$ express—via the time shifting property of the Fourier transform—the x and y shears of the interfering waves,

$$\Delta x = 2\left[\Delta z\tan(\Theta_B) - \frac{f_x t_M \Delta_M}{K_z}\right], \tag{23d}$$

$$\Delta y = \frac{2f_y[(t_M - z_M)\Delta_{21} - \Delta_M\Delta z] + \Delta f_y(\mathcal{A}_0 + t_A z_F)}{K_z}, \tag{23e}$$

where z_F is the focus distance from the splitter, see Fig. 2. Positive shears mean that the wave coming from the second interferometer arm (red in Fig. 2) precedes, in the positive x and y directions, the wave coming from the first. We note that the pooled forces defocus the interferometer and displace the interfering beams also in the absence of geometric aberrations.

In a skew-symmetric interferometer, neutrons fall differently in the two interferometer arms. Therefore, in addition to the defocus Δz, the differential fall

$$\Delta u_A = -\frac{2f_x t_M \Delta_M}{K_z} \tag{23f}$$

takes part in the x shear of the interfering waves.

The y shear originates jointly from the interferometer aberrations (defocus and different mirror thicknesses) and Coriolis force (via the terms proportional to Δf_y). The last might be significant in a split-crystal skew-symmetric interferometer having long arms.

The last term,

$$\beta = 2f_z[(z_M - t_M)\Delta_{21} + \Delta z\Delta_M],$$

where $f_z = (f_{hz} + f_{oz})/2$ is the mean axial force, originates from the different axial momentum transferred by the pooled forces in an aberrated interferometer. Unless the case of a split-crystal interferometer with a very large skewness Δ_M, it is a second-order term and can be neglected.

To clearly understand the physics behind the phase difference $f_x\mathcal{A}_0$, we analyze an aberration-free interferometer from two different viewpoints. First, we integrate neutron momentum along the unperturbed trajectories, and then we examine the interferometer operation from the vantage point of the falling neutrons.

A. Path integrals

Relying on geometric optics, the standard way to calculate the phase accumulated in the interferometer arms is to integrate the wave number (the spatial derivative of the phase) over the unperturbed trajectories that fulfill the Bragg condition (base rays), which are identified by the $\mathbf{q} = 0$ modes.

First, we observe that, classically, the neutron trajectories recombine on the analyzer input, but the fastest neutron bypasses the slowest one mimicking a defocus $\Delta z = 2f_x\mathcal{A}_0/K$ [38]. However, in our formalism, neutrons live in the xy plane, and the z coordinate is a fictitious time. Therefore, no separation occurs in space (the xy plane) and time (the z optical axis).

Assuming ideal geometry and following the base rays, the incoming neutron is split, when $z = 0$, in two halves that propagate horizontally in opposite directions. The two halves stop when $z = z_{M1}$ and z_{M2} for a t_M duration and are back-reflected when $z = z_{M1} + t_M$ and $z_{M2} + t_M$. Eventually, they recombine when $z = z_{M1} + t_M + z_{A1} = z_{M2} + t_M + z_{A2}$.

The difference between the phases accumulated in the split trajectories is due to the momenta $\hbar f_x z$ and $\hbar f_{ny} z$ transferred by the pooled forces. Since $y = 0$ on the base rays, the needed integrations are carried out along the x axis and the $\hbar f_{ny} z$ momentum does not play any role.

With the adopted sign conventions, a neutron propagating in the positive x direction accumulates a negative phase, see (1a). Therefore, parametrizing the motion by z, the phase gained in the first interferometer arm is

$$\begin{aligned}\phi_1 = &-\int_0^{z_{M1}} f_x z\tan(\Theta_B)\mathrm{d}z \\ &+\int_0^{z_{A1}} f_x(z_{M1} + t_M + z)\tan(\Theta_B)\mathrm{d}z,\end{aligned}$$

and that gained in the second arm is

$$\phi_2 = +\int_0^{z_{M2}} f_x z \tan(\Theta_B)\mathrm{d}z - \int_0^{z_{A2}} f_x(z_{M2}+t_M+z)\tan(\Theta_B)\mathrm{d}z,$$

where we used $\mathrm{d}x = \pm\tan(\Theta_B)\mathrm{d}z$. After computing the integrals, the phase difference is

$$\phi_2 - \phi_1 = 2f_x(t_M z_M + z_{M1}z_{M2})\tan(\Theta_B) = f_x\mathcal{A}_0,$$

which is the same as (22).

B. Free-fall frame

It is instructive to describe the interferometer operation from the vantage point of the free-falling neutrons. In the crystal frame, gravity and Coriolis force bend the neutron paths. In the free-fall frame, the neutrons' motion is straight; they cross the interferometer along the same paths they would take if there were no forces. At the same time, the interferometer crystals accelerate.

Neglecting the acceleration, the transfer matrix propagating a neutron in a crystal moving horizontally at constant velocity is given in Appendix E 1. The result is the same as the propagation in a crystal that is not in the exact Bragg condition. The perceived offsets,

$$\theta_S = -\frac{f_x t_S}{2K_z},$$
$$\theta_{Mi} = \theta_S - \frac{f_x\left(t_S/2 + z_{Mi} + t_{Mi}/2\right)}{K_z},$$
$$\theta_{Ai} = \theta_{Mi} - \frac{f_x\left(t_{Mi}/2 + z_{Ai} + t_A/2\right)}{K_z},$$

are consistent with the $q_{xj} = K\theta_j$ offsets of the arguments of the transmission and reflection coefficients in Eqs. (19). Here, S, M1, M2, and A indicate the splitter, mirrors, and analyzer, respectively, and $i = 1, 2$ indicates the interferometer arm. These angles are opposite to the deflections $f_x z_X/K_z$, where z_X is the distance of the X crystal centroid from the splitter input. For instance, in the case of the M1 mirror, $z_{M1} = t_S + z_{M1} + t_{M1}/2$. The crystal motion along the crystal vertical does not affect the neutron propagation.

Two remarks should be made: First, if the interferometer is free of geometrical aberrations, $\theta_{A2} = \theta_{A1}$ and the analyzer misalignment does not depend on the arm considered. Second, if the interferometer geometry is symmetric, i.e., $2\Delta_M = 0$, then $\theta_{M2} = \theta_{M1}$ and the mirrors are perceived as parallel. Contrary, if the geometry is skew-symmetric, i.e., $2\Delta_M \neq 0$, the mirrors are perceived to be misaligned by

$$\theta_{M2} - \theta_{M1} = -2f_x\Delta_M/K_z.$$

As regards the crystal displacements, the y component is irrelevant. The splitter, mirrors, and analyzer are seen displaced horizontally by (see Appendix E 2)

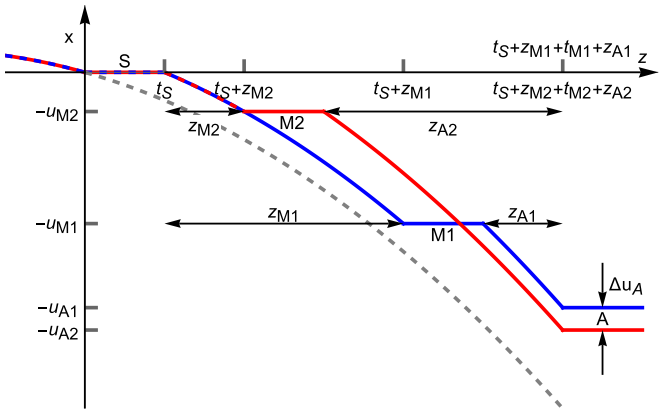

FIG. 3. Perturbations of the base rays due to the action of the pooled forces. The blue and red lines indicate the first and second interferometer arms, respectively. When the neutron traverses a crystal, the perturbation comes to a halt, but its velocity continues to change. The dashed line is the perturbation in free space.

$$u_S = 0,$$
$$u_{Mi} = u_S - \frac{f_x\left(2t_S z_{Mi} + z_{Mi}^2\right)\tan(\Theta_B)}{h},$$
$$u_{Ai} = u_{Mi} - \frac{f_x\left[2(t_S + z_{Mi} + t_M)z_{Ai} + z_{Ai}^2\right]\tan(\Theta_B)}{h},$$

where we neglected the interferometer aberrations and set the splitter displacement to zero. As discussed in the Appendixes C 2 and D 4, the crystal propagation stops the neutron fall, and the diffracting planes are seen as stationary. Therefore, the crystals' input and output surfaces are equally displaced.

The analyzer displacement depends on what arm of the interferometer the neutron goes through, see Fig. 3. The difference,

$$\Delta u_A = u_{A2} - u_{A1} = \frac{4f_x t_M \Delta_M \tan(\Theta_B)}{h} = \frac{2f_x t_M \Delta_M}{K_z},$$

where we used $2K_z\tan(\Theta_B) = h$, is the same as that given in (23d). The sign is the opposite because, here, Δu_A is the difference of the analyzer displacements whereas, in (23d), Δx is the shear between the interfering base rays.

With the adopted sign conventions, each reflection changes the neutron phase by $\pm hu_X$, where the plus (minus) sign applies to the incoming o (h) state, see (C2) and Fig. 2. No phase delay occurs in the transmissions. For instance, by considering the outgoing o state, the absolute phase changes along the two interferometer arms are

$$\phi_2 = h(u_{M2} - u_S),\ \ \phi_1 = h(u_A - u_{M1}).$$

The phase difference is

$$\phi_{21} = \phi_2 - \phi_1 = h\left(u_{M1} + u_{M2} - u_S - \frac{u_{A1} + u_{A2}}{2}\right),$$

where we heuristically averaged the different analyzer displacements. Carrying out the computations, see Ref. [24],

we obtain

$$\phi_{21} = 2f_x(t_M z_M + z_{M1} z_{M2})\tan(\Theta_B) = f_x \mathcal{A}_0,$$

which is the same as (22).

VI. INTERFERENCE SIGNAL

At the interferometer output port, free-space propagation separates the o and h states leaving the interferometer into two spatially localized states, $[\psi_{o1}(\mathfrak{x}) + \psi_{o2}(\mathfrak{x})]|o\rangle$ and $[\psi_{h1}(\mathfrak{x}) + \psi_{h2}(\mathfrak{x})]|h\rangle$, whose $i = 1, 2$ components interfere. Traveling fringes can be observed by varying the optical lengths of the interferometer arms, rotating the interferometer about the incoming (horizontal) beam, or altering the spacing or the Bragg angle alignment of the crystals of a split-crystal interferometer.

If the detectors count the total particles per time unit the observed signals are

$$I_n = \int_{-\infty}^{+\infty} |\psi_{n1}(\mathfrak{x}) + \psi_{n2}(\mathfrak{x})|^2 \mathrm{d}\mathfrak{x} = J_n[1 + \Gamma_n \cos(\phi_n)], \tag{24}$$

where $n = o, h$, $\widetilde{\psi}_{ni}(\mathfrak{x})$ are the position representations of the propagated wave functions (19), and the radius of the initial single-particle wave functions is equal to the (transverse) coherence length of the source.

By using the Parseval theorem and assuming infinite detectors, we can carry out the integration in the momentum space. Hence,

$$J_n = \sum_{i=1,2} \int_{-\infty}^{+\infty} \left|\widetilde{\psi}_{ni}(\mathbf{q})\right|^2 \mathrm{d}\mathbf{q}, \tag{25a}$$

$$\Xi_n = \int_{-\infty}^{+\infty} \widetilde{\psi}_{n2}(\mathbf{q}) \widetilde{\psi}^*_{n1}(\mathbf{q}) \mathrm{d}\mathbf{q}, \tag{25b}$$

$$\Gamma_n = 2|\Xi_n|/J_n, \tag{25c}$$

$$\phi_n = \arg(\Xi_n), \tag{25d}$$

where the star indicates complex conjugation.

By comparing (19a) with (19b), we see that, omitting gravity and Coriolis force, maximum visibility is achieved when the interferometer is free of geometric aberration; that is, $t_S = t_A$, $t_{M1} = t_{M2}$, and $z_{A1} = z_{M2}$, $z_{A2} = z_{M2}$.

The interference term can be written as

$$\Xi_n = \exp[\mathrm{i}(f_x \mathcal{A}_0 + f_x \mathcal{A}_1 + h\Delta u + \beta)] \times \int_{-\infty}^{+\infty} \mathrm{e}^{\mathrm{i}(q_x \Delta x + q_y \Delta y)} \mathbb{X}^*_{1n}(\mathbf{q}) \mathbb{X}_{2n}(\mathbf{q}) |\widetilde{\psi}_{\mathrm{in}}(\mathbf{q})|^2 \mathrm{d}\mathbf{q}, \tag{26}$$

where $\mathbb{X}_{1n}(\mathbf{q})$ and $\mathbb{X}_{2n}(\mathbf{q})$ are the products of the coefficients describing the neutron transmission or reflection by the crystals met along the $i = 1, 2$ arms, see Eqs. (19).

In Ref. [24] we show that

$$\frac{\mathbb{X}^*_{1o}\mathbb{X}_{2o}}{\mathbb{X}^*_{1h}\mathbb{X}_{2h}} = \mathrm{e}^{\mathrm{i}\pi}, \tag{27}$$

which proves that $\arg(\Xi_o)$ and $\arg(\Xi_h)$ differ by π.

Since $\mathbb{X}_{1n}(\mathbf{q})$ and $\mathbb{X}_{2n}(\mathbf{q})$ are independent of q_y, if $\widetilde{\psi}_{\mathrm{in}}(\mathbf{q})$ is separable, the integration over q_y in (25a) and (25b) gives $J_{ny} = \text{const}$ and

$$\Xi_{ny} = \int_{-\infty}^{+\infty} \mathrm{e}^{\mathrm{i}q_y \Delta y} |\widetilde{\psi}_{\mathrm{in}}(q_y - q_{yn})|^2 \mathrm{d}q_y = \exp\left(\mathrm{i} f_y z_D \Delta y - \frac{\Delta^2 y}{2\ell_0^2}\right), \tag{28}$$

where we assumed a Gaussian initial state with a radius equal to the coherence length ℓ_0 and omitted second-order terms. From (25c) it follows that the Δy shear of the interfering beams causes a loss of the fringe visibility depending on the source coherence.

Eventually, since $\mathbb{X}_{1n}(\mathbf{q})$ and $\mathbb{X}_{2n}(\mathbf{q})$ depend on the pooled forces, the dynamical diffraction contributes to the fringe phase via the argument of the integral in (26).

VII. CONCLUSIONS

We have been prompted to study the effect of gravity and Coriolis forces in crystal interferometers by a twofold motivation. First, the measured value of the gravitational phase shift of the interference pattern was found different from the theoretical prediction. Since there is no scientific basis for this difference, it must arise from a neglected effect in the interferometer operation. Second, in an on-the-way effort to design, realize, and operate a split-crystal interferometer operating simultaneously with x rays and neutrons, we need to master a detailed model of its operation.

We modeled the interferometer by relying on the momentum states and describing the neutron propagation analytically in terms of the transfer matrix propagating the plane-wave modes of the input single-particle wave packet. This is the usual approach to dynamical problems in quantum mechanics [39] and Bragg atom interferometry [40], and it is known as Fourier optics in optics [41]. Compared with the previous analyses [3,15–17,33,42], the Sagnac effect is now integral to the equations governing dynamical diffraction in the interferometer crystals.

Here we have introduced the transfer matrices for the propagation in free space and perfect crystals under the action of gravity and Coriolis force. They simplify the study of multicrystal systems, whose transfer matrix can be built by assembling them. We were limited to coherent Gaussian illuminations, but our results can be extended to other initial wave packets or partially coherent sources and include monochromators.

If the interferometer geometry is free from aberrations, the phase shift due to gravity and Coriolis force is proportional to their projection on the normal to the diffracting planes and the area of the loop by which the neutron wave function is returned to the splitter after recombined by the analyzer.

We found that, in aberrated interferometers, gravity and Coriolis forces make additional contributions to the neutron phase not previously considered though, compared with the present uncertainty, they might be negligible.

The interferometer defocus makes a phase contribution proportional to the area of the loop by which the recombined neutron returns to the focus after reaching the detector. It

might be significant if the detector is placed far from the interferometer.

If the mirrors' thicknesses do not equal that of the splitter and analyzer, the neutron perceives the mirrors' displacements as different from those of the splitter and analyzer. This difference makes a phase shift between the interfering waves.

Eventually, the gravity and Coriolis force shear the interfering waves proportionally to the interferometer skewness. The difference in the longitudinal acceleration of the o and h states shifts the phase of the crystals' reflection and transmission coefficients.

Neglecting the aberrations, we gave surrogate descriptions of the interferometer operation. First, relying on geometric optics, we re-obtained the phase accumulated in each interferometer arm by integrating the wave number over the arms' length. This is the standard way the phase shift between the interfering waves is calculated.

Second, from the vantage point of the falling neutron, the interferometer mirrors and analyzer tilt and displace. Therefore, we can switch off gravity and Coriolis force and explain the phase differences they induce in terms of these tilts and displacements. This model sheds further light on interferometer physics, simplifies its description, and might help to investigate the effect of seismic noise (of natural origin and man-made) in terms of differential displacements of the crystals.

Propagation in a magnetic field having a constant gradient is equivalent to propagation under gravity [31]. Therefore, our formalism can be extended to this case by pooling the resultant force and keeping track of the neutron spin states.

ACKNOWLEDGMENTS

Funding was received from the Austrian Research Promotion Agency (FFG Project No. FO999896034) and the Ministero dell'Istruzione, dell'Università e della Ricerca. Quantum Austria subsidies are financed from the Austrian Recovery and Resilience Fund "Next Generation EU." The theoretical model, analytic calculations, and numerical simulations were developed by C.P.S. and G.M. E.M. proposed using a split-crystal interferometer for vertical operation and conducted the experimental work that led to this investigation. All authors participated in discussing the results and contributed to the final paper. The authors thank H. Lemmel for fruitful discussions.

APPENDIX A: REPRESENTATIONS OF THE NEUTRON STATE

This Appendix clarifies the sign and normalization conventions used for the Fourier transform. The position and momentum representations of the single-particle state $|\psi_n(z)\rangle$ are the superpositions

$$\langle \mathfrak{x}|\psi_n(z)\rangle = \psi_n(\mathfrak{x};z) = \frac{1}{2\pi}\int_{-\infty}^{+\infty} \widetilde{\psi}_n(\mathbf{q};z)\mathrm{e}^{-\mathrm{i}\mathbf{q}\cdot\mathfrak{x}}\mathrm{d}\mathbf{q},$$

and

$$\langle \mathbf{q}|\psi_n(z)\rangle = \widetilde{\psi}_n(\mathbf{q};z) = \frac{1}{2\pi}\int_{-\infty}^{+\infty} \psi_n(\mathfrak{x};z)\mathrm{e}^{+\mathrm{i}\mathbf{q}\cdot\mathfrak{x}}\mathrm{d}\mathfrak{x}.$$

The orthogonality and completeness of the $\langle \mathfrak{x}|\mathbf{q}\rangle = \mathrm{e}^{+\mathrm{i}\mathbf{q}\cdot\mathfrak{x}}/(2\pi)$ and $\langle \mathbf{q}|\mathfrak{x}\rangle = \mathrm{e}^{-\mathrm{i}\mathbf{q}\cdot\mathfrak{x}}/(2\pi)$ bases are expressed by the integral representations of the delta distribution

$$\langle \mathbf{q}|\mathbf{q}'\rangle = \delta(\mathbf{q}'-\mathbf{q}) = \frac{1}{4\pi^2}\int_{-\infty}^{+\infty} \mathrm{e}^{\mathrm{i}(\mathbf{q}'-\mathbf{q})\cdot\mathfrak{x}}\mathrm{d}\mathfrak{x},$$

and

$$\langle \mathfrak{x}|\mathfrak{x}'\rangle = \delta(\mathfrak{x}-\mathfrak{x}') = \frac{1}{4\pi^2}\int_{-\infty}^{+\infty} \mathrm{e}^{\mathrm{i}\mathbf{q}\cdot(\mathfrak{x}-\mathfrak{x}')}\mathrm{d}\mathbf{q}.$$

With the convention adopted for the Fourier transform, the Fourier transform of $F(\mathfrak{x}) = f(\mathfrak{x})g(\mathfrak{x})$ is the convolution

$$\widetilde{F}(\mathbf{q}) = \frac{1}{2\pi}(\widetilde{f} * \widetilde{g})(\mathbf{q}) = \frac{1}{2\pi}\int_{-\infty}^{+\infty} \widetilde{f}(\mathbf{q}')\widetilde{g}(\mathbf{q}-\mathbf{q}')\mathrm{d}\mathbf{q}'.$$

APPENDIX B: POOLED FORCES

This Appendix explicitly gives the pooling of gravity and Coriolis force. With some abuse of language, we are terming it a force. Its dimensions are those of a squared wave number, but, as the optical axis z is identified with a fictitious time axis, $\mathbf{f}_n$ plays the role of a force.

Observing that, apart from the $2\hbar$ scale factor, the Coriolis force is

$$\Omega\mathbf{K}_n = K_z[\omega_y\hat{\mathbf{x}} - [\omega_x \mp \omega_z\tan(\Theta_B)]\hat{\mathbf{y}} \mp \omega_y\tan(\Theta_B)\hat{\mathbf{z}}],$$

where $n = o, h$ labels the neutron state, the pooling of gravity and Coriolis forces can be explicitly written as

$$\begin{aligned}\mathbf{f}_n = \frac{m^2}{\hbar^2 K_z}\Bigg\{&\left(g_x - \frac{2\hbar K_z\omega_y}{m}\right)\hat{\mathbf{x}}\\ &+\left(g_y + \frac{2\hbar K_z[\omega_x \mp \omega_z\tan(\Theta_B)]}{m}\right)\hat{\mathbf{y}}\\ &+\left(g_z \pm \frac{2\hbar K_z\omega_y\tan(\Theta_B)}{m}\right)\hat{\mathbf{z}}\Bigg\}.\end{aligned}$$

It is worth noting that the x component of $\mathbf{f}$ is independent of the neutron state.

The mean and span of the o to h values are

$$\begin{aligned}\mathbf{f} = \frac{\mathbf{f}_o + \mathbf{f}_h}{2} = \frac{m^2}{\hbar^2 K_z}\Bigg\{&\left(g_x - \frac{2\hbar K_z\omega_y}{m}\right)\hat{\mathbf{x}}\\ &+\left(g_y + \frac{2\hbar K_z\omega_x}{m}\right)\hat{\mathbf{y}} + g_z\hat{\mathbf{z}}\Bigg\},\end{aligned}$$

and

$$\Delta\mathbf{f} = \frac{\mathbf{f}_h - \mathbf{f}_o}{2} = -\frac{2m\omega_z\tan(\Theta_B)}{\hbar}\hat{\mathbf{y}} + \frac{2m\omega_y\tan(\Theta_B)}{\hbar}\hat{\mathbf{z}}.$$

By using $\omega = 72.7\times10^{-6}$ rad/s, $\lambda = 0.272$ nm, $\Theta_B = \pi/4$ rad, the magnitude of the Coriolis acceleration is $2\hbar K_z\omega/m = 0.15\ \mathrm{m/s^2}$, to be compared with the acceleration due to the gravity, $g = 9.81\ \mathrm{m/s^2}$. Also, $f \approx 1.51\times10^5\ \mathrm{m^{-2}}$ and $\Delta f \lesssim 2.3\times10^3\ \mathrm{m^{-2}}$.

APPENDIX C: UNPERTURBED TRAJECTORIES

This Appendix gives the unperturbed trajectories of the o and h modes in free space and of the guided modes in perfect crystals.

1. Free space

In the Heisenberg picture, identifying the optical axis z as the time axis, the time-dependent position operator is $\mathfrak{x}_H(z) = F_0(z)^\dagger \mathfrak{x}_S F_0(z)$, where $\mathfrak{x}_S$ is the (time-independent) position operator in the Schrödinger picture. Therefore, the unperturbed neutron trajectories of the o and h modes in free space are given by the expectation value of Ref. [43]

$$\begin{aligned}\mathfrak{x}_H(\mathbf{q};z) &= \widetilde{F}_0^\dagger(\mathbf{q};z)[-\mathrm{i}\boldsymbol{\nabla}_{\mathbf{q}}\widetilde{F}_0(\mathbf{q};z)] \\ &= \begin{bmatrix} z\mathbf{q}/K_z + \tan(\Theta_B)z\hat{\mathbf{x}} & 0 \\ 0 & z\mathbf{q}/K_z - \tan(\Theta_B)z\hat{\mathbf{x}} \end{bmatrix},\end{aligned} \tag{C1}$$

where [by setting $\mathbf{f} = (0,0,0)$] the momentum representations of $F_0(z)$ and $\mathfrak{x}_S$ are (17) and $-\mathrm{i}\boldsymbol{\nabla}_{\mathbf{q}}$, respectively, and we exploited the diagonality of both to omit the relevant Dirac deltas.

Since the transfer matrix $F_0(z)$ is independent of q_y, the y component of $\mathfrak{x}_H(\mathbf{q};z)$ is null and neutrons propagate along the x axis. The first term of (C1), $z\mathbf{q}/K_z$, takes the deviation from the Bragg condition into account. The second term, $\pm z\tan(\Theta_B)\hat{\mathbf{x}}$, gives the horizontal displacements of the o and h states with velocities $\pm\tan(\Theta_B)$.

The unperturbed trajectories fulfilling the Bragg conditions

$$\langle \mathfrak{x}_H(z)\rangle = \pm z\tan(\Theta_B)\hat{\mathbf{x}}$$

are associated with the $\mathbf{q} = 0$ modes or the $\langle\mathbf{q}\rangle = (0,0)$ wave functions; that is, to wave functions having a symmetric momentum distribution.

2. Perfect crystal

Identifying z as time, the neutron trajectory in a perfect crystal can be calculated by propagating $\mathfrak{x}_S$ in the same way as in the free space. Hence, $\mathfrak{x}_H(z) = U_0(z)^\dagger \mathfrak{x}_S U_0(z)$. Omitting gravity and Coriolis force, the momentum representation of the propagator,

$$\widetilde{U}_0(\mathbf{q},\mathbf{q}';z) = \begin{bmatrix} T(\eta;z) & \mathrm{e}^{-\mathrm{i}hu}R(\eta;z) \\ \mathrm{e}^{+\mathrm{i}hu}R(\eta;z) & T(-\eta;z) \end{bmatrix}\delta(\mathbf{q}-\mathbf{q}'), \tag{C2}$$

is given by (12b) where $\mathbf{f} = (0,0,0)$ and $\overline{u} = u$ is the (horizontal) crystal displacement, if any.

The trajectories of the (not normalized) guided modes,

$$|\pm,\mathbf{q}\rangle = \begin{bmatrix} \eta \pm \sqrt{1+\eta^2} \\ -1 \end{bmatrix}, \tag{C3}$$

are

$$\begin{aligned}\langle \mathbf{q},\pm|\mathfrak{x}_H(z)|\pm,\mathbf{q}\rangle &= \langle\pm,\mathbf{q}|\widetilde{U}_0^\dagger(\mathbf{q};z)[-\mathrm{i}\boldsymbol{\nabla}_{\mathbf{q}}\widetilde{U}_0(\mathbf{q};z)]|\mathbf{q},\pm\rangle \\ &= \pm\frac{\eta\tan(\Theta_B)z}{\sqrt{1+\eta^2}}\hat{\mathbf{x}},\end{aligned} \tag{C4}$$

where $\widetilde{U}_0(\mathbf{q};z) = \widetilde{U}_0(\mathbf{q},\mathbf{q};z)$. Since the transfer matrix is independent of q_y, the y component of the position operator is null and neutrons propagate in the reflection plane. The guided modes traverse the crystal at the angles $\pm\digamma(\eta)$ relative to the diffracting, where [33]

$$\tan(\digamma) = \frac{\eta\tan(\Theta_B)}{\sqrt{1+\eta^2}}. \tag{C5}$$

Eventually, the unperturbed trajectories in a perfect crystal are given by

$$\langle \mathfrak{x}_H(z)\rangle = \pm\int_{-\infty}^{+\infty}\widetilde{\psi}^*(\mathbf{q};0)\frac{\eta\tan(\Theta_B)z\hat{\mathbf{x}}}{\sqrt{1+\eta^2}}\widetilde{\psi}(\mathbf{q};0)\mathrm{d}\mathbf{q}.$$

If $\langle\mathbf{q}\rangle = (0,0)$, then $\langle\eta\rangle = 0$ and neutrons propagate parallel to the diffracting planes. In particular, this statement holds for the $\mathbf{q} = 0$ modes, which correspond to the base rays.

APPENDIX D: PERTURBED TRAJECTORIES

Here we provide the trajectories, affected by gravity and Coriolis forces, of the o and h modes in free space and of the guided modes in perfect crystals.

1. Free space: Exact Hamiltonian

First, we calculate the perturbed trajectory in free space by using the exact Hamiltonian (4), that is,

$$H_n = \frac{\hbar^2 k_n^2}{2m} - m\mathbf{g}\cdot\mathbf{r} - \hbar(\Omega\mathbf{r})\cdot\mathbf{k}_n. \tag{D1}$$

The Heisenberg equations of the motion for the canonical momentum and position operators are

$$\hbar\partial_\tau\mathbf{k}_n = \mathrm{i}[\mathbf{k}_n, H_n] = -\boldsymbol{\nabla}_{\mathbf{r}}H_n = m\mathbf{g} - \hbar(\Omega\mathbf{K}_n), \tag{D2a}$$

$$\hbar\partial_\tau\mathbf{r} = \mathrm{i}[\mathbf{r}, H_n] = \boldsymbol{\nabla}_{\mathbf{k}_n}H_n = \frac{\hbar^2\mathbf{k}_n}{m} - \frac{\hbar(\Omega\mathbf{K}_n)\tau}{m}. \tag{D2b}$$

Here, $\mathbf{k}_n = \mathbf{K}_n + \mathbf{p}$ and, in the last equations, we approximated $\mathbf{k}_n$ by $\mathbf{K}_n$ and $\mathbf{r}$ by the nth base ray $\mathbf{K}_n z'/K_z = \hbar\mathbf{K}_n\tau/m$. Also, we omitted the subscript H indicating the Heisenberg picture, used τ to indicate the time, and differentiated the third component of the perturbed and unperturbed trajectories as z and z', respectively.

Integrating (D2a) with $\mathbf{p}(0) = (0,0,0)$, the evolution of the momentum operator is

$$\mathbf{k}_n = \mathbf{K}_n + \frac{m^2\mathbf{g}z'}{\hbar^2K_z} - \frac{m(\Omega\mathbf{K}_n)z'}{\hbar K_z}, \tag{D3a}$$

where $z' = \hbar K_z\tau/m$ is the unperturbed distance traveled in the τ time.

Remembering the relationship between the kinetic, $m\boldsymbol{\upsilon}_n = m(\mathbf{V}_n + \mathbf{v})$, and canonical, $\hbar\mathbf{k}_n$, momenta, and observing that

$$m\boldsymbol{\upsilon}_n = \hbar\mathbf{k}_n - m(\Omega\mathbf{r}) \approx \hbar\mathbf{k}_n - m(\Omega\mathbf{K}_n)z'/K_z$$
$$= \hbar\mathbf{K}_n + \frac{m^2\mathbf{g}z'}{\hbar K_z} - \frac{2m(\Omega\mathbf{K}_n)z'}{K_z}, \tag{D3b}$$

where $\mathbf{r} \approx \mathbf{K}_n z'/K_z$ are the base rays, we can see that (D3a) recovers the change of the kinetic momentum correctly.

Using (D3a) in (D2b), where $\partial_\tau = m\partial_z/(\hbar K_z)$, and integrating over z with $\mathbf{r}(0) = (0, 0, 0)$, the evolution of the position operator is

$$\mathbf{r} = \frac{\mathbf{K}_n z'}{K_z} + \frac{m^2\mathbf{g}z'^2}{2\hbar^2 K_z^2} - \frac{m(\Omega\mathbf{K}_n)z'^2}{\hbar K_z^2}. \tag{D3c}$$

The first term in (D3c) replicates the nth base ray. The remaining ones are the perturbations due to gravity and the Coriolis force.

2. Free space: Approximate Hamiltonian

To verify the approximations made, we now solve again the equations of motion (D2a) and (D2b) by using the approximate Hamiltonian in (5), which is

$$H_n = \frac{\hbar^2}{2m}\left(k_n^2 - 2K_z\mathbf{f}_n \cdot \mathbf{r}\right). \tag{D4}$$

The initial conditions are $\mathbf{p}(0) = (0, 0, 0)$ and $\mathbf{r}(0) = (0, 0, 0)$. The canonical momentum and position operators evolve according to (see Ref. [24] for the derivation)

$$\mathbf{k}_n = \mathbf{K}_n + \mathbf{f}_n z' = \mathbf{K}_n + \frac{m^2\mathbf{g}z'}{\hbar^2 K_z} - \frac{2m(\Omega\mathbf{K}_n)z'}{\hbar K_z}, \tag{D5a}$$

$$\mathbf{r} = \frac{\mathbf{K}_n z'}{K_z} + \frac{\mathbf{f}_n z'^2}{2K_z} = \frac{\mathbf{K}_n z'}{K_z} + \frac{m^2\mathbf{g}z'^2}{2\hbar^2 K_z^2} - \frac{m(\Omega\mathbf{K}_n)z'^2}{\hbar K_z^2}. \tag{D5b}$$

Equation (D5b) is the same as (D3c). When comparing (D5a) with (D3a), we must observe that the Hamiltonian (D4) is independent of the neutron velocity $\boldsymbol{\upsilon}_n$. Therefore, kinematical momentum $m\boldsymbol{\upsilon}_n$ now equals the canonical momentum $\hbar\mathbf{k}_n$. Hence,

$$m\boldsymbol{\upsilon}_n = \hbar\mathbf{k}_n = \hbar\mathbf{K}_n + \frac{m^2\mathbf{g}z'}{\hbar K_z} - \frac{2m(\Omega\mathbf{K}_n)z'}{K_z}, \tag{D6}$$

which is the same as (D3b). It is worth noting that this identity is ensured by the factor of two in the Coriolis term $\mathbf{f}_n \cdot \mathbf{r}$.

3. Free space: Transfer matrix

To further test the correctness of the transfer matrix in (8a)–(8c), we now derive the evolution of the position operator via $\mathfrak{x}_H(z) = F(z)^\dagger \mathfrak{x}_S F(z)$, in the same way as we did in Sec. C 1. Since $\widetilde{F}(\mathbf{q}, \mathbf{q}'; z)$ is not diagonal, we must make explicit that the momentum representation of the momentum operator is diagonal. Hence, $\mathfrak{x}_S(\mathbf{q}, \mathbf{q}') = -\mathrm{i}\delta(\mathbf{q} - \mathbf{q}')\nabla_{\mathbf{q}}$.

To make the algebra the simplest, we consider the propagation along the crystal vertical. Hence, the evolution of the position operator is (see Ref. [24] for the detailed derivation)

$$y_H(q_y, q_y'; z) = \int_{-\infty}^{+\infty} \widetilde{F}_{ym}^\dagger(q_y, q_y''; z)[-\mathrm{i}\partial_{q_y''}\widetilde{F}_{yn}(q_y'', q_y'; z)]\mathrm{d}q_y''$$
$$= \left(\frac{q_y z}{K_z} + \delta_n y\right)\delta(q_y - q_y'),$$

where $\widetilde{F}_{ny}^\dagger(q_y, q_y''; z) = \widetilde{F}_{ny}^*(q_y'', q_y; z)$ and we exploited its diagonality to omit the relevant Dirac deltas. The first term, $q_y z/K_z = \hbar q_y \tau/m$, is the displacement in the $z = \hbar K_z \tau/m$ time due to the initial velocity $\hbar q_y/m$. The second term, $\delta_n y = f_{ny} z^2/(2K_z)$, is the fall in the same time due to the acceleration $\hbar^2 K_z f_{ny}/m^2$.

4. Crystal

To calculate the perturbed trajectories in a perfect crystal, we need to write the Hamiltonian in (11) as

$$H = \frac{\hbar^2 K_z}{m}[q_x \tan(\Theta_B)\sigma_3 - (\mathfrak{f} \cdot \mathbf{r})\sigma_0 - \upsilon\sigma_1], \tag{D7}$$

where σ_j are the Pauli matrices [44], σ_0 is the 2×2 unit matrix, $\mathfrak{f} = (f_x, f_y)$, we neglected the difference between the Coriolis force acting on the o and h states, multiplied both sides of (11) by $\hbar^2 K_z/m$, and identified $(\hbar^2 K_z/m)\partial_z$ with $\hbar\partial_\tau$.

Solving the equation of the motion (D2a) and (D2b) with $\mathbf{q}_H(0) = \mathbf{q}_0\sigma_0$ and $\mathfrak{x}_H(0) = (0, 0)\sigma_3$, the evolutions of the momentum and position operators is

$$\mathbf{q}_H(z) = (\mathbf{q}_0 + \mathfrak{f}z)\sigma_0, \tag{D8a}$$

$$x_H(z) = z\tan(\Theta_B)\hat{\mathbf{x}}\sigma_3. \tag{D8b}$$

Since the Hamiltonian (D7) is independent of q_y (owing to the first-order approximation the kinetic term $\hbar^2 q^2\sigma_0/(2m)$ has been omitted), the y component of the position operator, $y_H(z) = 0$, is a constant of the motion. For the same reason, in (D8b), the $q_{0x} z\sigma_0/K_z$ term is missing. The $\exp[-\mathrm{i}q^2 z/(2K_z)]$ factor has been added to the transfer matrix $\widetilde{U}(\mathbf{q}, \mathbf{q}'; z)$ in (12b) to correct this faulty consequences.

The expected values of the momentum and position of the guided modes (C3) are

$$\langle \mathbf{q}, \pm|\mathbf{q}_H(z)|\pm, \mathbf{q}\rangle = \mathbf{q}_0 + \mathfrak{f}z, \tag{D9a}$$

$$\langle \mathbf{q}, \pm|x_H(z)|\pm, \mathbf{q}\rangle = \frac{\eta(\eta \pm \sqrt{1+\eta^2})\tan(\Theta_B)z}{1 + \eta(\eta \pm \sqrt{1+\eta^2})}$$
$$\approx \pm\frac{\eta\tan(\Theta_B)z}{\sqrt{1+\eta^2}}, \tag{D9b}$$

where the approximation made holds about $\eta = 0$ to the order η^3.

The discussion that follows (C4) is still relevant: The guided propagation prevents the neutron from falling along the x axis. It is important to note that the deviation from the unperturbed path comes from the (second order) kinetic-energy term of Hamiltonians (D1) and (D4). Thus, the absence

of deviation results from the first-order approximation used to obtain (D7). We should take note that the conflicting velocity changes, $\hbar f_x t/m$ and $\hbar f_y t/m$, persist because they are first-order effects.

APPENDIX E: FREE-FALL FRAME

This Appendix supports the description of the interferometer operation using a freely falling frame, where the neutron motion is straight, but the interferometer crystals accelerate. First, neglecting the acceleration, we calculate the transfer matrix propagating the neutron through a crystal moving at constant velocity. Next, we calculate the displacements of the accelerating crystals when the neutron reaches them.

1. Galilei boost

Let $-\mathbf{v}_0$ be the instantaneous velocity of a generic interferometer crystal (splitter, mirror, or analyzer) as seen in the free-fall frame. The operator making the Galilean transformation of the quantum state taking the position vector $\mathbf{r}' = \mathbf{r} - \mathbf{v}_0\tau$ in the free-fall frame into $\mathbf{r}$ in the crystal frame is [29,45,46]

$$\begin{aligned}\widetilde{\psi}'(\mathbf{q};z') &= \mathrm{e}^{\mathrm{i}p_{z0}z}\int_{-\infty}^{+\infty} G(\mathbf{q},\mathbf{q}')\widetilde{\psi}(\mathbf{q}';z)\mathrm{d}\mathbf{q}' \\ &= \mathrm{e}^{\mathrm{i}p_{z0}z}\widetilde{\psi}(\mathbf{q}+\mathbf{q}_0;z),\end{aligned} \tag{E1}$$

where $\hbar\mathbf{p}_0 = m\mathbf{v}_0 = \hbar(\mathbf{q}_0, p_{z0})$.

Therefore, in the momentum space, the desired operator is represented by

$$G(\mathbf{q},\mathbf{q}') = \delta(\mathbf{q}'-\mathbf{q}-\mathbf{q}_0), \tag{E2}$$

and the transfer matrix of the moving crystal is

$$\begin{aligned}\widetilde{U}'(\mathbf{q},\mathbf{q}';t) &= \int_{-\infty}^{+\infty} G^{-1}(\mathbf{q},\mathbf{q}'')\widetilde{U}_0(\mathbf{q}'';t)G(\mathbf{q}'',\mathbf{q}')\mathrm{d}\mathbf{q}'' \\ &= \widetilde{U}_0(\mathbf{q}-\mathbf{q}_0;t),\end{aligned} \tag{E3}$$

where the transfer matrix of the perfect crystal $\widetilde{U}_0(\mathbf{q};z) = \widetilde{U}_0(\mathbf{q},\mathbf{q};z)$ is given by (C2).

The transfer matrix $\widetilde{U}'(\mathbf{q},\mathbf{q}';t)$ propagates the neutron in a perfect crystal that is rotated about the crystal vertical by the angle [37]

$$\theta = -q_{0x}/K_z. \tag{E4}$$

2. Crystal displacements

In the free-fall frame, indicating by z_B the gap between two generic interferometer crystals A and B, the horizontal displacement of B's input,

$$\begin{aligned}u_B &= u_A - \frac{mv_A z_B}{\hbar K_z} - \frac{f_x z_B^2}{2K_z} \\ &= u_A - \frac{2q_A z_B\tan(\Theta_B)}{h} - \frac{f_x z_B^2\tan(\Theta_B)}{h},\end{aligned} \tag{E5}$$

is opposite to the horizontal fall in the $\tau_B = mz_B/(\hbar K_z)$ time, see Fig. 3.

As shown by the discussion following (D9b) and (C4) and in Fig. 3, the propagation in a crystal occurs parallel to the diffracting planes. Therefore, no crystal motion occurs in the transit and the displacements of the input and output faces are the same. For this reason, in (E5), u_A is the displacement of both A's input and output.

According to (D9a), the horizontal velocity at A's output (also known as the instantaneous velocity of its output surface as seen by the falling neutron) is changed to $v_A = v_0 + \hbar f_x t_A/m = \hbar q_A/m$, where v_0 is the input velocity and t_A is the thickness. Therefore, the second term of (E5) is opposite to the neutron displacement in the τ_B time because of this initial velocity. The last term is the fall because of the acceleration $f_x\hbar^2K_z/m^2$, see (7). Eventually, we used the relationship $2K_z\tan(\Theta_B) = h$.

Setting the displacement of the splitter (input and output) to zero and applying (E5), the mirrors' displacements are

$$u_{Mi} = -\frac{f_x\left(2t_S z_{Mi} + z_{Mi}^2\right)\tan(\Theta_B)}{h},$$

where we used $u_S = 0$, $v_0 = 0$, and $q_S = f_x t_S$. The analyzer displacement,

$$u_{Ai} = u_{Mi} - \frac{f_x\left[2(t_S + z_{Mi} + t_{Mi})z_{Ai} + z_{Ai}^2\right]\tan(\Theta_B)}{h},$$

is again obtained by application of (E5), where $u_A = u_{Mi}$ and $q_A = f_x(t_S + z_{Mi} + t_M)$. It is worth noting that, as shown in Fig. 3, the displacement of the analyzer depends on which arm, $i = 1, 2$, is traveled.

APPENDIX F: DEFINITIONS

Symbols have been defined at their first occurrence. However, since our subsequent paper [13] consistently uses the same symbols and to avoid readers having to go back and forth to search for each symbol, Table I provides a list of symbols.

TABLE I. List of the main symbols.

$\hat{\mathbf{x}}$	Normal to the diffracting planes (horizontal)	$\hat{\mathbf{y}}$	Normal to the reflection plane (vertical)
$\hat{\mathbf{z}}$	Normal to the crystal surface (optical axis)	$\mathbf{r} = (\mathfrak{x}, z)$	Position vector
$\mathfrak{x} = (x, y)$	$\mathbf{r}$ component orthogonal to $\hat{\mathbf{z}}$	$\mathbf{h} = -2\pi\hat{\mathbf{x}}/d$	Reciprocal vector
d	Diffracting plane spacing	$\mathbf{K}_o$, $\mathbf{K}_h$	Kinematical wave vectors, see (2)
$\mathbf{p} = (\mathbf{q}, p_z)$	Wave vectors' deviation from $\mathbf{K}_{oh}$, see (3a)	$\mathbf{q} = (q_x, q_y)$	Variable conjugate to $\mathfrak{x}$
$\mathbf{k}_n = \mathbf{K}_n + \mathbf{p}$	Wave vectors of the $\mathbf{q}$ modes	Θ_B	Bragg angle, see (2)
$\gamma = \cos(\Theta_B)$	Director cosine	$2K\sin(\Theta_B) = h$	Bragg law
$K_z = K\cos(\Theta_B)$	z component of $\mathbf{K}_{o,h}$	$K_x = K\sin(\Theta_B)$	x component of $\mathbf{K}_{o,h}$ (modulus)
m	Neutron mass	$\hbar$	Reduced Planck's constant
$\boldsymbol{\omega} = (\omega_x, \omega_y, \omega_z)$	Earth's angular velocity, see (4)	Ω	matrix representation of $\boldsymbol{\omega}\times$
$\mathbf{g} = (g_x, g_y, g_z)$	Acceleration due to gravity	$2\hbar(\Omega\mathbf{K}_n)$	Coriolis force (approximation)
$\hbar^2 K_z \mathbf{f}_n/m$	Pooled forces, see (7)	$\mathbf{f} = (\mathbf{f}_h + \mathbf{f}_o)/2$	Mean of the pooled forces
$2\Delta\mathbf{f} = \mathbf{f}_h - \mathbf{f}_o$	Difference of the pooled forces	$\mathfrak{f}_n = (f_x, f_{ny})$	$\mathbf{f}_n$ projection in the xy plane
$\delta_n\mathbf{p} = \mathbf{f}_n z$	Transferred momenta, see (9a)	$\delta_n\mathbf{r} = (\delta_n\mathbf{p})z$	Base-ray perturbations, see (9b)
$-K^2\chi_{0,h}$	Fermi pseudopotential (Fourier components)	$\overline{u}$	Effective lattice displacement, see (14a)
ℓ_0	Coherence length	$\upsilon = \chi_{\pm h}K/(2\gamma)$	Coupling coefficient, see (11)
$\zeta = \pi z/\Lambda_e$	Dimensionless propagation distance, see (13a) and (13b)	$\eta = \Lambda_e\tan(\Theta_B)p/\pi$	Dimensionless resonance error, see (13a) and (13b)
$\Lambda_e = \lambda\gamma/\lvert\chi_h\rvert$	*Pendellösung* length	$t_S, t_{\mathrm{M1}}, t_{\mathrm{M2}}, t_A$	Crystal thicknesses
$t_M = (t_{\mathrm{M1}} + t_{\mathrm{M2}})/2$	Mean mirror thickness	$2\Delta_{21} = t_{\mathrm{M2}} - t_{\mathrm{M1}}$	Differential mirror thickness
$z_M = (z_{\mathrm{M1}} + z_{\mathrm{M2}})/2$	Mean mirror distance	$2\Delta_M = z_{\mathrm{M2}} - z_{\mathrm{M2}}$	Skewness, see (20b)
Δz	Defocus, see (23a)	Δx, Δy	Interfering-wave shear, see (23d)–(23f)
$\mathcal{A}_0$, $\mathcal{A}_1$	Areas of the interferometer and detector loops, see (21) and (23b)		
θ	Rotation angle about $\hat{\mathbf{y}}$, see (14b)	$\lvert\psi_{\mathrm{in}}\rangle$, $\lvert\psi_{\mathrm{out}}\rangle$	Initial and final states, see (16a)
$\widetilde{\psi}_n(\mathbf{q}; z)$	Partial Fourier transform of $\psi_n(\mathfrak{x}; z)$, see (3b)		
$R(\eta; z)$, $T(\eta; z)$	Reflection and transmission coefficients, see (13a) and (13b)	$U(z)$, $F(z)$, X_1, X_2	Transfer matrices, see (12b), (17), (16b), and (16c)
$n = o, h$	State components (label)	$i = 1, 2$	Interferometer arm (label)

[1] R. Colella, A. W. Overhauser, and S. A. Werner, Observation of gravitationally induced quantum interference, Phys. Rev. Lett. **34**, 1472 (1975).

[2] J. L. Staudenmann, S. A. Werner, R. Colella, and A. W. Overhauser, Gravity and inertia in quantum mechanics, Phys. Rev. A **21**, 1419 (1980).

[3] S. Werner, H. Kaiser, M. Arif, and R. Clothier, Neutron interference induced by gravity: New results and interpretations, Physica B + C (Amsterdam) **151**, 22 (1988).

[4] K. C. Littrell, B. E. Allman, and S. A. Werner, Two-wavelength-difference measurement of gravitationally induced quantum interference phases, Phys. Rev. A **56**, 1767 (1997).

[5] U. Bonse and M. Hart, An x-ray interferometer, Appl. Phys. Lett. **6**, 155 (1965).

[6] H. Rauch, W. Treimer, and U. Bonse, Test of a single crystal neutron interferometer, Phys. Lett. A **47**, 369 (1974).

[7] H. Lemmel, M. Jentschel, H. Abele, F. Lafont, B. Guerard, C. P. Sasso, G. Mana, and E. Massa, Neutron interference from a split-crystal interferometer, J. Appl. Crystallogr. **55**, 870 (2022).

[8] G. L. Greene and V. Gudkov, Neutron interferometric method to provide improved constraints on non-Newtonian gravity at the nanometer scale, Phys. Rev. C **75**, 015501 (2007).

[9] A. Saha, Colella-Overhauser-Werner test of the weak equivalence principle: A low-energy window to look into the noncommutative structure of space-time? Phys. Rev. D **89**, 025010 (2014).

[10] C. Marletto and V. Vedral, Gravitationally induced entanglement between two massive particles is sufficient evidence of quantum effects in gravity, Phys. Rev. Lett. **119**, 240402 (2017).

[11] F. Hammad, A. Landry, and K. Mathieu, Prospects for testing the inverse-square law and gravitomagnetism using quantum interference, Int. J. Mod. Phys. D **30**, 2150004 (2021).

[12] J. M. Rocha and F. Dahia, Neutron interferometry and tests of short-range modifications of gravity, Phys. Rev. D **103**, 124014 (2021).

[13] E. Massa, G. Mana, and C. P. Sasso, following paper, Gravitational and Coriolis forces in crystal neutron interferometry. II. Numerical simulations, Phys. Rev. A **110**, 062819 (2024).

[14] D. M. Greenberger and A. W. Overhauser, Coherence effects in neutron diffraction and gravity experiments, Rev. Mod. Phys. **51**, 43 (1979).

[15] U. Bonse and T. Wroblewski, Dynamical diffraction effects in noninertial neutron interferometry, Phys. Rev. D **30**, 1214 (1984).

[16] M. A. Horne, Neutron interferometry in a gravity field, Physica B + C (Amsterdam) **137**, 260 (1986).
[17] B. Heacock, M. Arif, R. Haun, M. G. Huber, D. A. Pushin, and A. R. Young, Neutron interferometer crystallographic imperfections and gravitationally induced quantum interference measurements, Phys. Rev. A **95**, 013840 (2017).
[18] H. Rauch and S. A. Werner, *Neutron Interferometry: Lessons in Experimental Quantum Mechanics*, Oxford Series on Neutron Scattering in Condensed Matter (Clarendon Press, Oxford, 2000).
[19] H. Abele and H. Leeb, Gravitation and quantum interference experiments with neutrons, New J. Phys. **14**, 055010 (2012).
[20] G. Mana and F. Montanari, A Fourier optics approach to the dynamical theory of x-ray diffraction—perfect crystals, Acta Crystallogr., Sect. A: Found. Crystallogr. **60**, 40 (2004).
[21] G. Mana and E. Vittone, LLL x-ray interferometry: I. Theory, Z. Phys. B: Condens. Matter **102**, 189 (1997).
[22] See Supplemental Material at http://link.aps.org/supplemental/10.1103/PhysRevA.110.062818 for the algebraic and analytical steps (part 1) and the symbolic computation (part 2).
[23] Wolfram Research, Inc., *Mathematica, Version 13.3* (Champaign, IL, 2023).
[24] Wolfram Research, Inc., Wolfram Player, Version 12.3.1 (Champaign, IL, 2023).
[25] A. Authier, *Dynamical Theory of X-Ray Diffraction*, IUCR Crystallographic Symposia Series (Oxford University Press, New York, NY, 2001).
[26] L. S. Brown and Y. Zhang, Path integral for the motion of a particle in a linear potential, Am. J. Phys. **62**, 806 (1994).
[27] G. P. Arrighini, N. L. Durante, and C. Guidotti, More on the quantum propagator of a particle in a linear potential, Am. J. Phys. **64**, 1036 (1996).
[28] B. R. Holstein, The linear potential propagator, Am. J. Phys. **65**, 414 (1997).
[29] J. Anandan, Jeevaand Suzuki, Quantum mechanics in a rotating frame, in *Relativity in Rotating Frames: Relativistic Physics in Rotating Reference Frames*, edited by G. Rizzi and M. L. Ruggiero (Springer Netherlands, Dordrecht, 2004), pp. 361–370.
[30] E. Benedetto, I. Bochicchio, C. Corda, F. Feleppa, and E. Laserra, Generalized potential for apparent forces: The Coriolis effect, Eur. J. Phys. **41**, 045002 (2020).
[31] S. A. Werner, Gravitational and magnetic field effects on the dynamical diffraction of neutrons, Phys. Rev. B **21**, 1774 (1980).
[32] G. Mana and C. Palmisano, A Fourier optics approach to the dynamical theory of x-ray diffraction—continuously deformed crystals, Acta Crystallogr., Sect. A: Found. Crystallogr. **60**, 283 (2004).
[33] K. C. Littrell, B. E. Allman, O. I. Motrunich, and S. A. Werner, The effects of dynamical diffraction on the measurement of gravitationally induced quantum phase shifts by neutron interferometry, Acta Crystallogr., Sect. A: Found. Crystallogr. **54**, 563 (1998).
[34] C. P. Sasso, G. Mana, and E. Massa, Crystal bending in triple-Laue x-ray interferometry. Part I. Theory, J. Appl. Crystallogr. **56**, 707 (2023).
[35] H. Lemmel, Comment on "Relativistic effects in atom and neutron interferometry and the differences between them" by Greenberger, Schleich, and Rasel, arXiv:1406.1328.
[36] C. P. Sasso, G. Mana, and E. Massa, Three-dimensional model of a split-crystal x-ray and neutron interferometer, J. Appl. Crystallogr. **55**, 1500 (2022).
[37] C. P. Sasso, G. Mana, and E. Massa, A skew-symmetric split-crystal neutron and x-ray interferometer, J. Appl. Crystallogr. **57**, 44 (2024).
[38] H. Lemmel (private communication).
[39] D. J. Griffiths and C. A. Steinke, Waves in locally periodic media, Am. J. Phys. **69**, 137 (2001).
[40] J.-N. Siemß, F. Fitzek, S. Abend, E. M. Rasel, N. Gaaloul, and K. Hammerer, Analytic theory for Bragg atom interferometry based on the adiabatic theorem, Phys. Rev. A **102**, 033709 (2020).
[41] J. Goodman, *Introduction to Fourier Optics*, McGraw-Hill Physical and Quantum Electronics Series (Roberts and Company Publishers, Englewood, Co, 2005).
[42] J. Springer, M. Zawisky, H. Lemmel, and M. Suda, A neutron interferometric measurement of a phase shift induced by Laue transmission, Acta Crystallogr., Sect. A: Found. Crystallogr. **66**, 17 (2010).
[43] A. Tokmakoff, Schrödinger and Heisenberg Representations (University of Chicago, IL, 2020), online, accessed 2023-06-02.
[44] L. Tisza, The Pauli Algebra (Massachusetts Institute of Technology, MA, 2021), online, accessed 2023-06-09.
[45] W. Klink, Quantum mechanics in noninertial reference frames, Ann. Phys. (NY) **260**, 27 (1997).
[46] S. Weinberg, *Lectures on Quantum Mechanics*, 2nd ed. (Cambridge University Press, Cambridge, 2015).